Final Report on AFOSR-Funded Research Project

(September 2006)

Title: Fabrications of Photonic Bandgap Structures in Si and Ge Substrates Using Laser-assisted Nanoimprinting of Self-assembled Nanoparticles

Award Number: F49620-03-1-0426

Project Period: 15 AUG 2003 – 14 AUG 2006

Reported by:

Yongfeng Lu
Professor
Department of Electrical Engineering,
University of Nebraska Lincoln,
209N Walter Scott Engineering Center,
Lincoln, NE 68588-0511
Tel: 402-472-8323
Fax: 402-472-4732
Email: ylu2@unl.edu

REPORT DOCUMENTATION PAGE

Form Approved
OMB No. 0704-0188

1. REPORT DATE *(DD-MM-YYYY)*	2. REPORT TYPE	3. DATES COVERED *(From - To)*
	FINAL REPORT	15 AUG 2003 - 31 JUL 2006

4. TITLE AND SUBTITLE
FABRICATION OF PHOTONIC BANDGAP STRUCTURES IN SI AND SUBSTRATES USING LASER-ASSISTED NANOIMPRINTING OF SELF-ASSEMBLED NANOPARTICLES

5a. CONTRACT NUMBER

5b. GRANT NUMBER
F49620-03-1-0426

5c. PROGRAM ELEMENT NUMBER
61102F

6. AUTHOR(S)
PROFESSOR YONGFEING LU

5d. PROJECT NUMBER
2305/DX

5e. TASK NUMBER
DX

5f. WORK UNIT NUMBER

7. PERFORMING ORGANIZATION NAME(S) AND ADDRESS(ES)
UNIVERSITY OF NEBRASKA
OFFICE OF SPONSORED PROGRAMS
312 N 14TH STREET
LINCOLN NE 68588-0430

8. PERFORMING ORGANIZATION REPORT NUMBER

9. SPONSORING/MONITORING AGENCY NAME(S) AND ADDRESS(ES)
AIR FORCE OF SCIENCTIFIC RESEARCH
AFOSR/NE
875 NORTH RANDOLPH STREET
SUITE 325 ROOM 3112
ARLINGTON VA 22203-1768
Dr Gernot Pomrenke

10. SPONSOR/MONITOR'S ACRONYM(S)

11. SPONSOR/MONITOR'S REPORT NUMBER(S)
AFRL-SR-AR-TR-06-0490

12. DISTRIBUTION/AVAILABILITY STATEMENT
DISTRIBUTION STATMENT A: UNLIMITED

13. SUPPLEMENTARY NOTES

14. ABSTRACT

The fabrications of periodic dielectric structures at nanoscales, which are called photonic bandgap (PBG) structures, have attracted the interests of researchers due to the applications in a variety of fields such as optoelectronics, photonics, sensors, photo catalysts, and energy harvesting coatings. One- and two-dimensional PBG structures have been realized because such systems are very amenable to conventional fabrication techniques. However, three-dimensional (3-D) PBG structures are still remained as an important and motivating challenge. This project aimed at the fabrication of 3-D PBG structures with laser-assisted processing techniques. Theoretical simulation and experimental measurements for optical properties of PBG structures were also carried out. The morphologies, material properties, and optical properties of the PBG structures were characterized using scanning electron microscopy (SEM), Raman spectroscopy (RS), and spectroscopic ellipsometry (SE). It has been proved that 3-D PBG structures with expected optical properties can be obtained using laser-assisted processing techniques.

15. SUBJECT TERMS

16. SECURITY CLASSIFICATION OF:			17. LIMITATION OF ABSTRACT	18. NUMBER OF PAGES	19a. NAME OF RESPONSIBLE PERSON
a. REPORT	b. ABSTRACT	c. THIS PAGE			19b. TELEPHONE NUMBER *(Include area code)*
U	U	U			

Table of Content

1. Summary

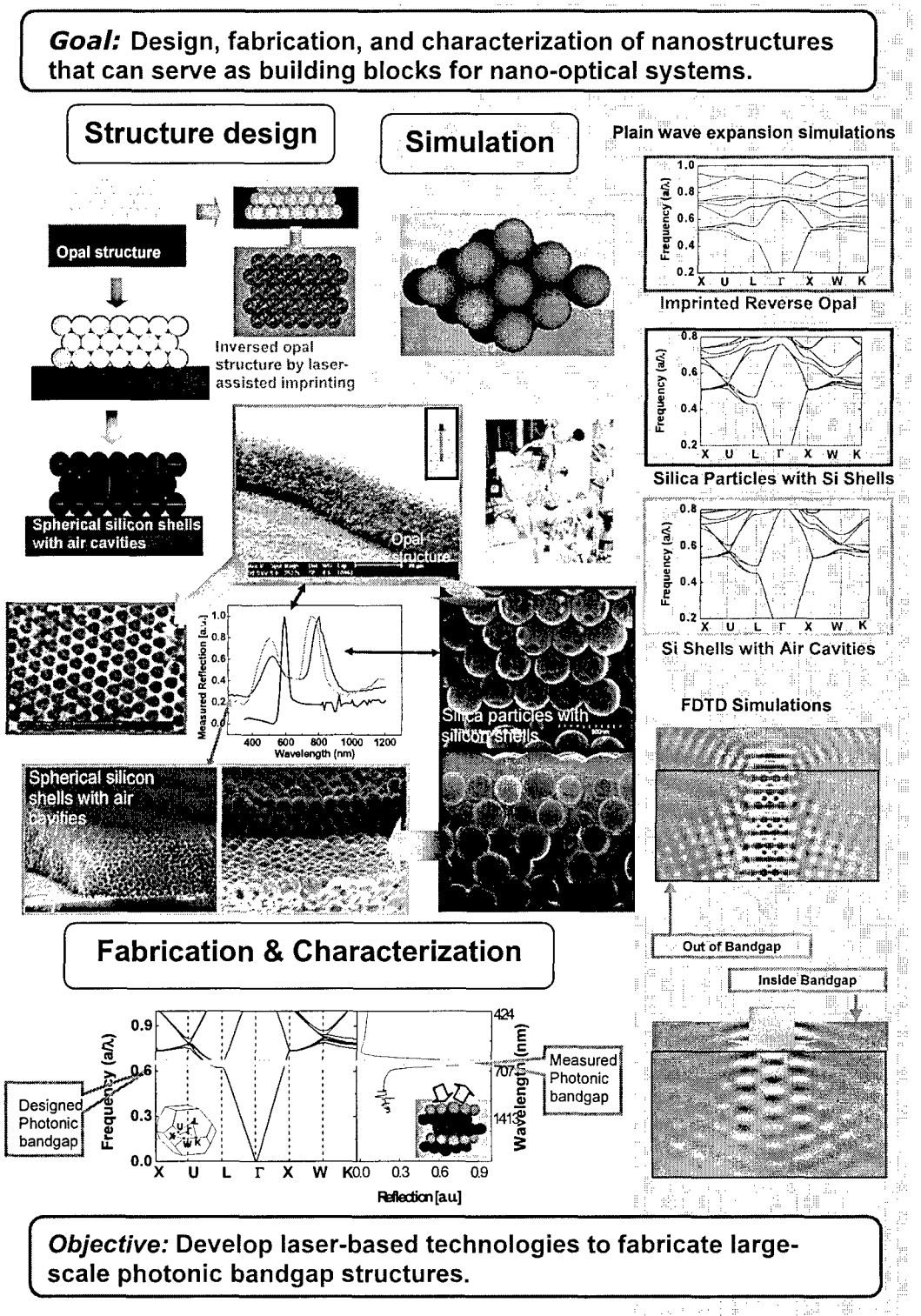

Figure 1. Overlook of the Project.

The fabrications of periodic dielectric structures at nanoscales, which are called photonic bandgap (PBG) structures, have attracted the interests of researchers due to the applications in a variety of fields such as optoelectronics, photonics, sensors, photo catalysts, and energy harvesting coatings. One- and two-dimensional PBG structures have been realized because such systems are very amenable to conventional fabrication techniques. However, three-dimensional (3-D) PBG structures are still remained as an important and motivating challenge. This project aimed at the fabrication of 3-D PBG structures with laser-assisted processing techniques. Theoretical simulation and experimental measurements for optical properties of PBG structures were also carried out. The morphologies, material properties, and optical properties of the PBG structures were characterized using scanning electron microscopy (SEM), Raman spectroscopy (RS), and spectroscopic ellipsometry (SE). It has been proved that 3-D PBG structures with expected optical properties can be obtained using laser-assisted processing techniques.

Self-assembly of silica particles, laser-assisted nanoimprinting, and laser-assisted chemical vapor deposition (LCVD) have been applied to fabricating PBG structures with complete photonic bandgaps. Simulations of the thermal process in laser-assisted nanoimprinting and optical properties of the fabricated PBG structures were carried out. The experimental results in characterizing the PBG structures agree well with the simulation results, indicating that the PBG structures were successfully obtained.

The whole structure of the project is shown in Fig. 1. In this report, we will categorize our research into two fabrication routes: laser-assisted nanoimprinting and LCVD, as shown in Fig. 2.

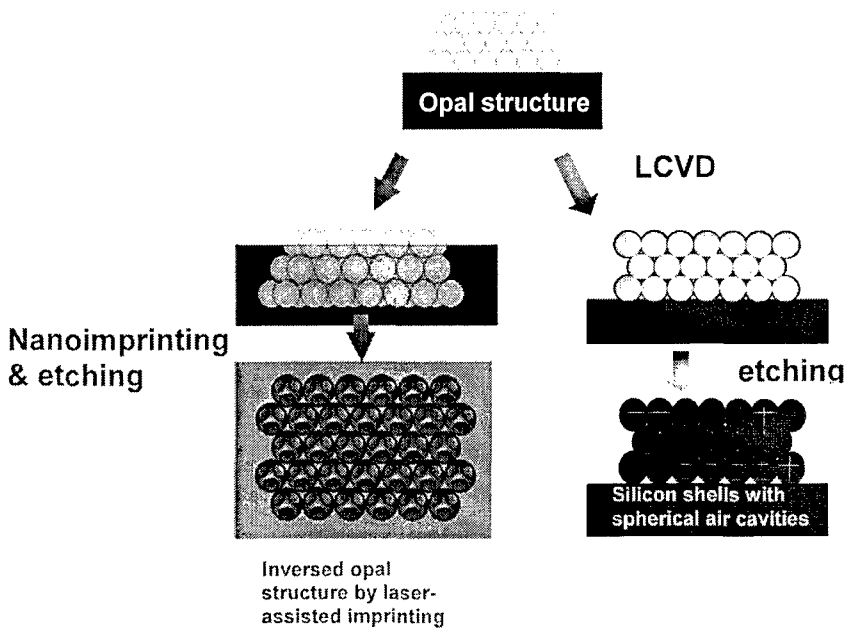

Figure 2. Fabrication routes.

2 Laser–assisted nanoimprinting

Since the development of laser-assisted nanoimprinting in 2002, it has been regarded as a promising approach to fabricating nanoscale structures. Laser-assisted nanoimprinting has received wide interest due to its extreme easiness and rapidity, as it needs only one excimer laser pulse (with a pulse duration of 10-20 ns) to imprint a pattern into a silicon substrate. In this work, we developed a method combining both the flexibility of particle self-assembly and the rapid process of laser-assisted nanoimprinting. In this section, we show that a monolayer or multiple layers of self-assembled silica particles can be imprinted into various substrates, including silicon and photoresist, with one or several pulses of excimer laser irradiation (Fig. 3). By removing the silica particles embedded in the substrates using hydrofluoric (HF) acid, inverse-opal photonic crystals were formed. Laser-assisted nanoimprinting has been proved to be an efficient way to infiltrate the self-assembly structures and fabricate ordered array of spherical cavities. This enabled us to explore the possibility of fabricating 3-D PBG structures with complete photonic bandgaps. Compared with other techniques for 3-D PBG fabrication, this method is faster, more cost effective, and simpler. We fabricated inverse-opal structures in silicon using laser-assisted nanoimprinting of silica particles with diameters in the range of 0.33-1.54 μm.

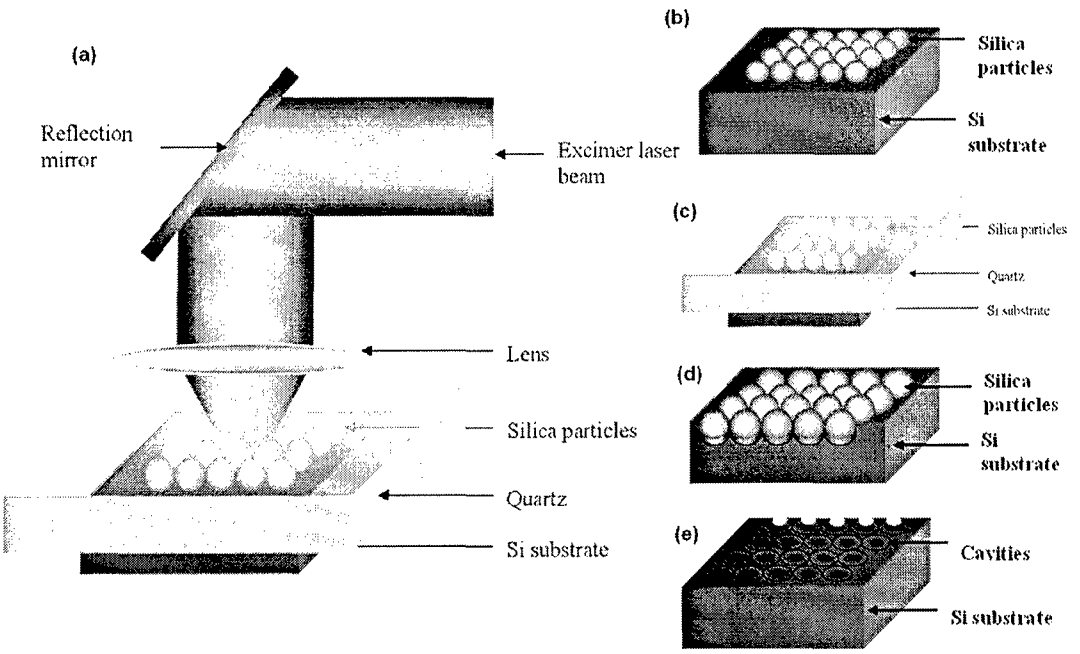

Figure 3. (a) Schematic diagram of the set up for laser-assisted nanoimprinting; (b) silica particle self-assembly on silicon substrate; (c) self-assembly sample with a quartz plate on it; (d) imprinted structure; (e) obtained inverse opal structure after HF etching.

2.1 Fabrication of 2-D photonic bandgap structures

The fabrication of 2-D PBG structures was begun with the tilt method for self-assembly, followed by laser-assisted nanoimprinting on various substrates, including silicon and photoresist. The monolayer of silica particles served not only as nanoimprinting molds, but also micro lenses which provided intensive optical field below each particle due to the near-field effects. The optical near-field effects in laser nanoimprinting were simulated with the high-frequency structure simulator (HFSS, Ansoft Inc.).

2.1.1 Self-assembly of silica particles with the tilt method

The tilt method was used to form a monolayer of self-assembled silica particles. After the substrates were completely cleaned, a surfactant (triton-X: methanol = 1:400) was dropped onto the tilted substrate surfaces. The substrates were left to dry at room temperature. The surfactant helped to wet the substrates. Suspensions of monodisperse silica particles (Bangs Laboratories, Inc.) were subsequently dispensed onto the substrates. The suspensions contain 10% solution silica (SiO_2) particles with diameters in a range from 0.33 to 1.54 μm. Hexagonal close-packed assemblies over an area around several hundred square microns was obtained (Fig. 4). The SEM micrographs of self-assembled monolayers of 0.97 and 1.54 μm silica particles are shown in Fig. 5.

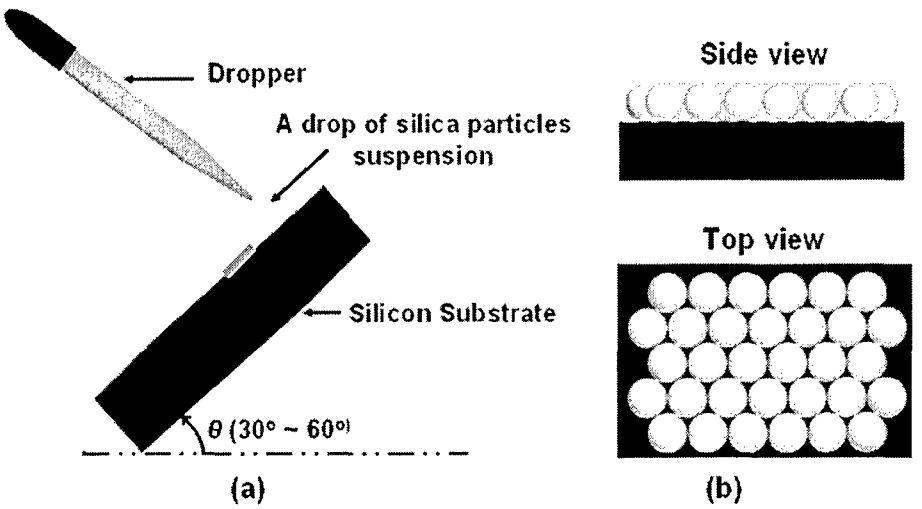

Figure 4. (a) Schematic diagram of the set up for self-assembly (b) schematic diagram of the top and side views of a monolayer of silica particles on Si substrates.

2.1.2 2-D nanoimprinting on photoresist polymers

We fabricated 2-D PBGs in photoresist polymer films. Silicon substrates were used to support the polymer films (IC28T3). A spin coater (Headway Research), which can spin up to a speed of 10,000 rpm, was used for coating the polymer films on silicon substrates. The structures formed in polymer films (0.6~ 2 μm thick) are shown in Figs. 6(a) and 6(b).

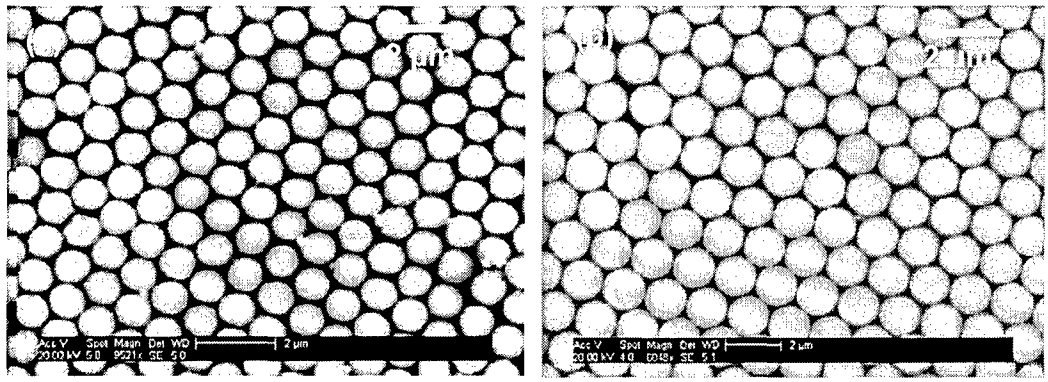

Figure 5. Self-assembled monolayers of (a) 0.97 μm and (b) 1.54 μm silica particles.

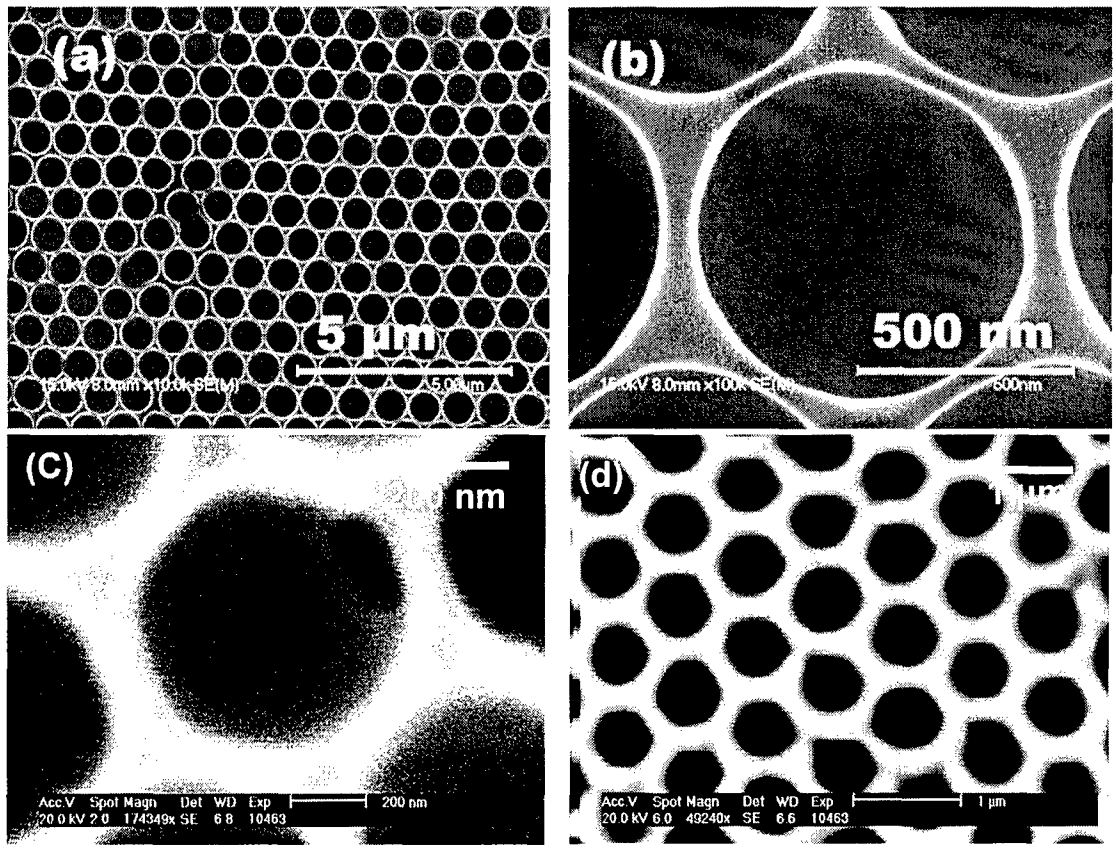

Figure 6. The SEM images of monolayer semi-spherical cavities in photoresist films under different magnifications.

2.1.3 2-D nanoimprinting on silicon substrates

In order to imprint the self-assembled silica particles into silicon substrates, a single pulse of KrF excimer laser (Lambda Physik Complex 205, wavelength = 248 nm, pulse duration = 23 ns), with a fluence of 0.8~1.0 J/cm^2 was vertically irradiated on the quartz plate placed on the silicon substrate containing the silica particles. After the irradiation of the KrF excimer laser, the silica

particles were imprinted into the substrates. The embedded particles were subsequently removed to obtain the hemispherical nano-cavities. The structures formed using 0.97 μm silica particles are shown in Fig. 7.

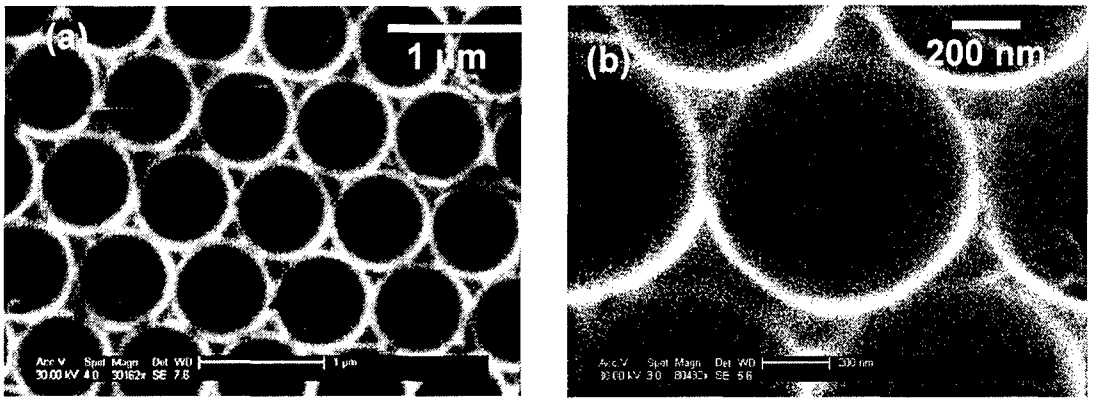

Figure 7. Hemispherical cavities formed by laser imprinting 0.97 μm silica particles on a silicon surface.

2.1.4 Optical simulation using high frequency structure simulator

In order to investigate the laser interactions with the silica particles and the substrates, we used the High Frequency Structure Simulator (HFSS, Ansoft Inc.) software to simulate the 3-D distribution of optical intensity. HFSS can be used to create 3-D models of the silica particles and the substrates, thereby allowing us to have a clear understanding of the laser propagation both within the particles and at the contact points between the particles and the substrates. We simulated the optical intensity distribution in a silica particle of 0.8 μm diameter placed inside an air box. The incident wave was a laser beam with a wavelength of 248 nm which normally irradiates on the silica particles from the top of the air box. It is assumed that the wave propagates along the negative Z direction, hence the directions of the electric field and magnetic field are along the X and Y axes, respectively. The incident magnitude of the electric field is 10 V/m. Figures 8 shows the simulation results of the optical field distribution in Y-Z plane cross the center of the spherical particle and X-Y plane where the particle touches the substrate, as indicated in the insets. It is found that the intensity of the electric field increases about 7 times with respect to the incident wave after the wave goes through the silica particle. The simulation results indicated that for monolayer nanoimprinting, near-field effect was an important factor which enhanced the laser intensity at the bottom of each particle.

2.2 Fabrication of 3-D photonic bandgap structures

Laser-assisted imprinting was also employed for imprinting multiple layers of self-assembled silica particles. Thereby a fabrication technique to build 3-D photonic crystals was developed. After obtaining a monolayer self-assembly of hexagonally-closely packed silica particles, the self-assembly process was repeated on the same sample to obtain multiple layers of self-assembled silica particles as shown in Fig. 9(a). The schematic diagrams of the top view and the side view of a double-layer assembly of silica particles on a Si substrate are shown in Fig. 9(b).

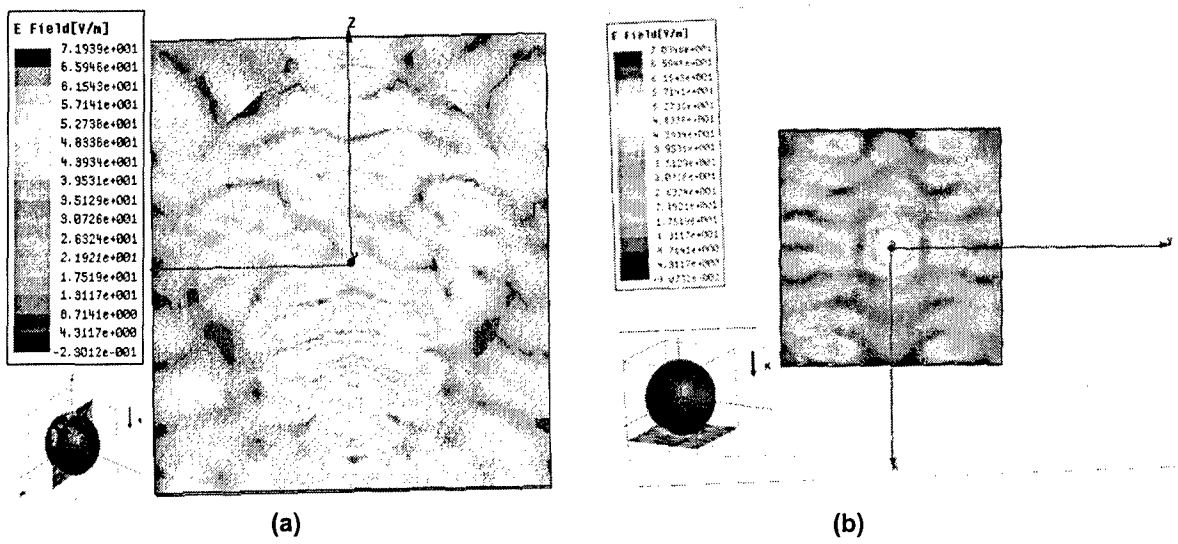

Figure 8. Simulation results of the electric field distribution in different planes for a laser beam (248 nm) propagating through a 0.8 μm silica particle with an incident magnitude E_0 = 10 V/m: (a) X-Z plane, (b) the particle-substrate contacting X-Y plane.

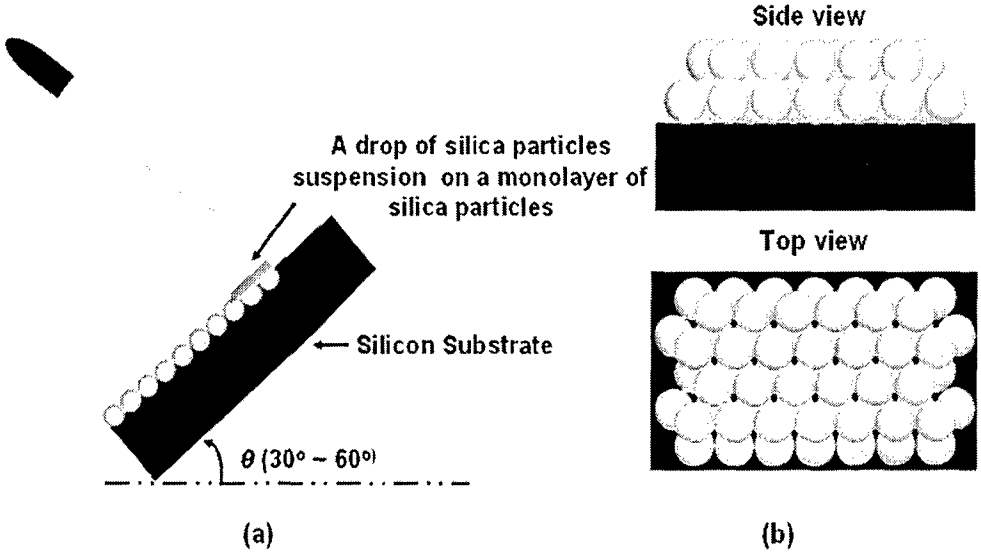

Figure 9. (a) Schematic diagram of the set up for multiple layer self-assembly (b) schematic diagrams of the top and side views of two layers of silica particles on a substrate surface.

The laser-assisted imprinting setup is shown in Fig. 10. A Si substrate which contains the multiple layers of silica particles was placed on a hot plate and preheated to 550 ^{o}C. The temperature of the Si substrate was measured using a thermo-coupler. A single pulse of KrF excimer laser was irradiated on a quartz plate placed on the as-prepared sample. Since quartz plate is transparent to the UV laser, applying external force on the quartz plate helps to imprint the silica particles into the molten Si during laser irradiation. The fluences used in this study

were in a range from 1 to 1.5 Jcm^{-2}. During imprinting, molten Si covered the imprinted silica particles. The schematic picture of this is shown in Fig. 11.

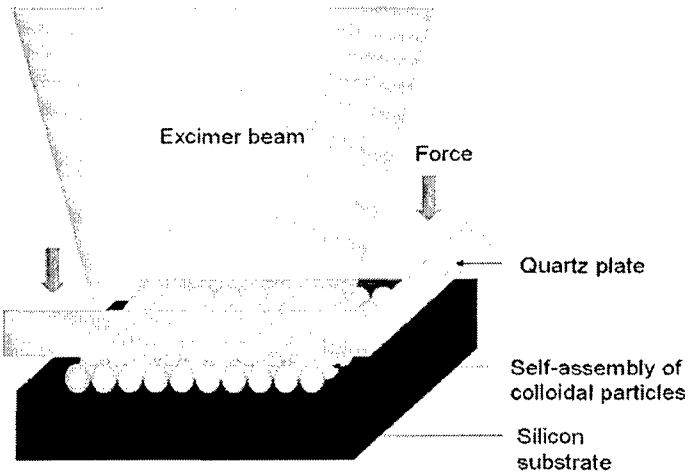

Figure 10. Experimental setup for laser-assisted imprinting of multilayer self-assembled silica particles.

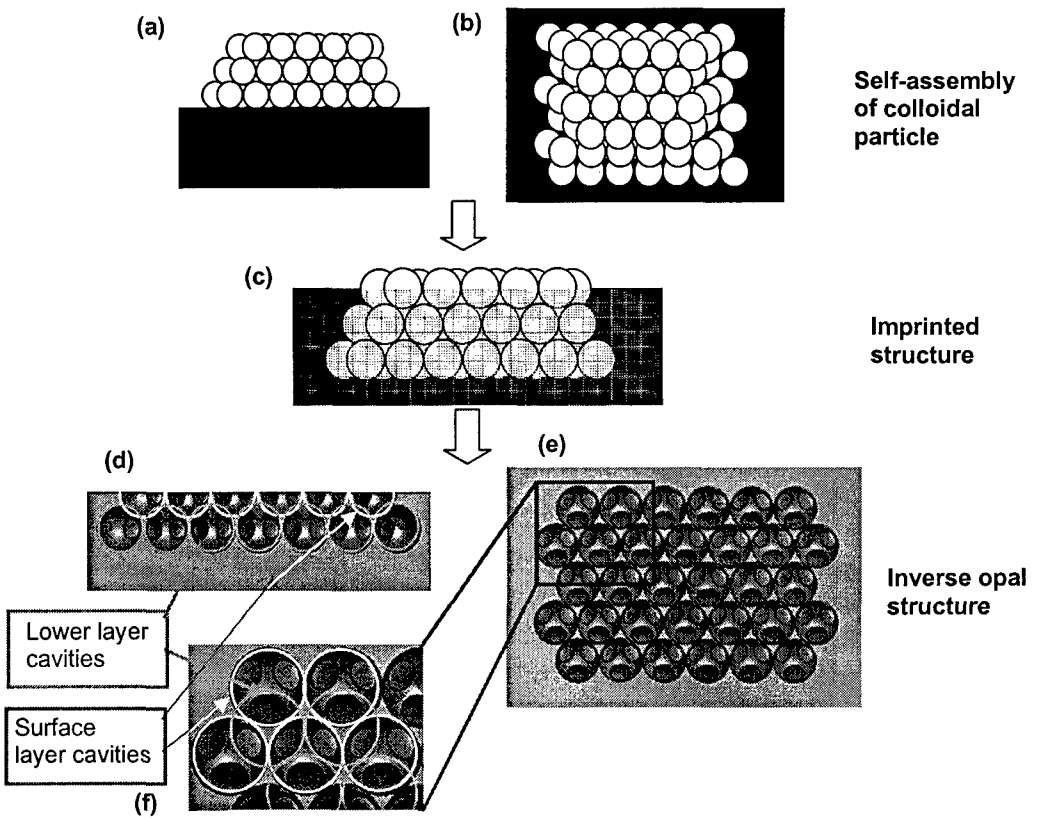

Figure 11. Schematic diagrams of PBG structures obtained after each processing step in laser-assisted imprinting route. (a) side view of self-assembled structure; (b) top view of self-assembled structure; (c) side view of imprinted structure; (d) side view of inverse opal structure after HF etching; (e) top view of inverse opal structure; and (f) close up of (e).

In order to obtain 3-D inverse opal structures, the sample was then cleaned ultrasonically to remove the silica particles remaining on the substrate and then etched with HF acid which removes the embedded silica microparticles by dissolving them. The schematic diagrams of the cross-sectional view and the top-view of the inverse opals formed in the Si substrate after removing the imprinted silica particles are shown in Figs. 11(d) and 11(e). In Fig. 11(d), the cross cut portion gives an idea of the internal structure of an inverse opal.

2.2.1 3-D nanoimprinting on silicon substrates

The successful laser imprinting of monolayer silica particles in silicon enabled us to explore the possibilities of imprinting multiple-layered silica particles. Figures 12(a)-(d) show the structures formed on silicon surfaces by multiple-layer imprinting of 0.97 μm silica particles.

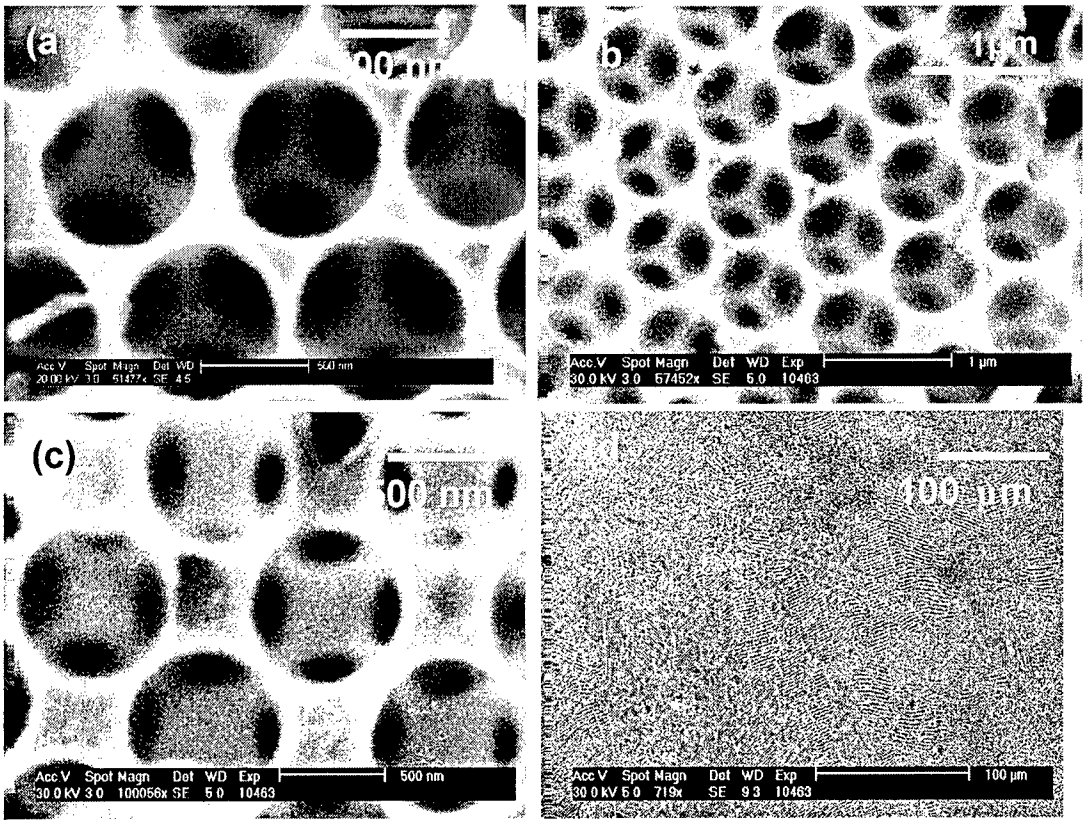

Figure 12. (a), (b) Structures formed by imprinting multiple layers of 0.97 μm silica particles under different magnifications with a <111> orientation; (c) the structures formed are in an orientation of <100>, which is not quite commonly observed; (d) large area of the structures formed by the nanoimprinting of multiple layers of 0.97 μm silica particles.

2.2.2 3-D nanoimprinting on photoresist films

In an effort to test multilayer imprinting for its applicability to different materials, multilayer imprinting has also been employed on polymer films. Since the polymer has lower thermal stability, 3 laser pulses with a fluence of 500 mJ/cm^2 were applied. Figure 13 shows the SEM micrographs of inverse opals structures formed after imprinting silica particles with a size of 0.81 μm in polymer films.

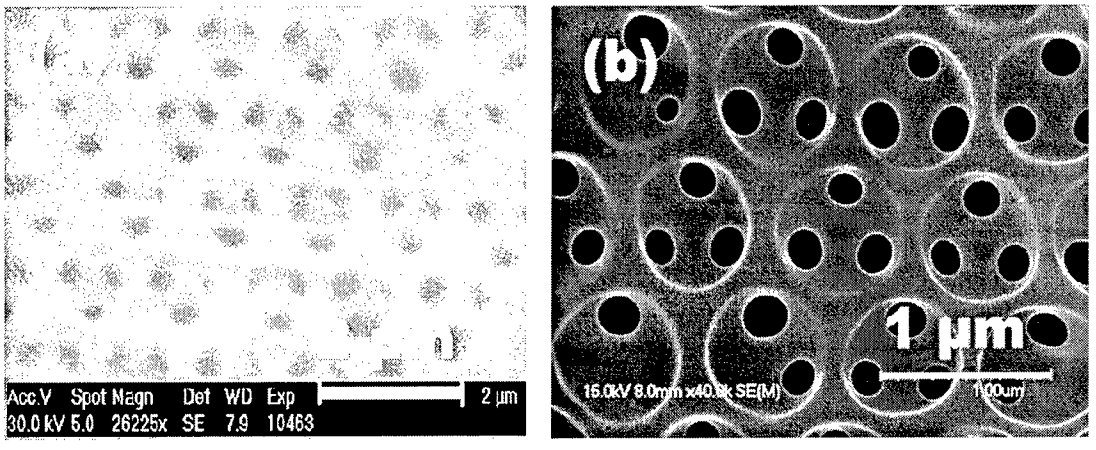

Figure 13. The SEM images of 3-D spherical cavities under different magnifications.

2.2.3 Simulations of laser interaction with materials

In order to optimize the laser parameters and substrate temperatures, the Simulation of Laser Interaction with Materials (SLIM) was used to calculate the temperature distribution during the imprinting process.

In the calculation for the surface temperature and the melting depth of Si, five different laser fluences from 0.69 to 2 J/cm^2 were taken. Figure 14 shows the surface temperatures of a Si substrate during the laser irradiation under different laser fluences as a function of time. Figure 15 shows the melting depths of a Si substrate during laser irradiation under different laser fluences. In order to optimize the nanoimprinting parameters, the thermal calculation were also carried out for different substrate preheating temperatures. The laser fluence is 1 J/cm^2. Figure 16 shows the surface temperature of Si substrate as a function of time during the laser irradiation with a fluence of 1 J/cm^2 and with different initial substrate temperatures ranging from 300 to 900 K. Figure 17 shows the maximum melting depth of the sample as a function of initial substrate temperature in a range from 300 to 900 K. Substrates with higher initial substrate temperatures have larger maximum melting depths. Therefore, silica particles are more likely to be imprinted into melted Si substrates with higher preheating temperatures.

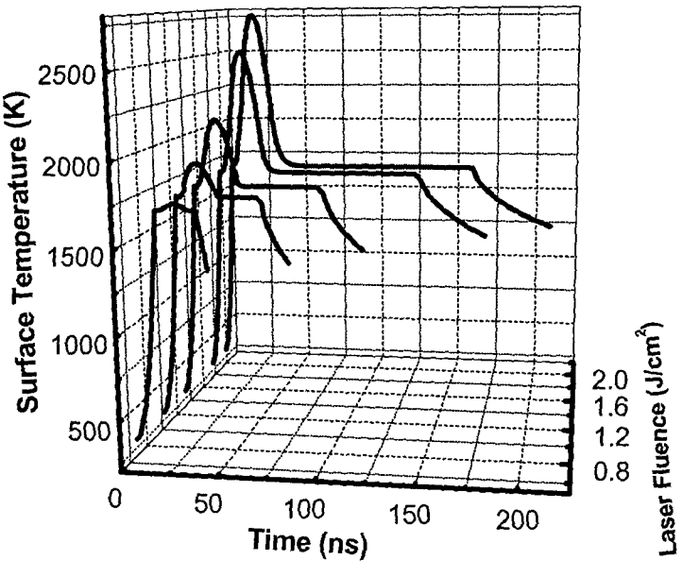

Figure 14. Surface temperatures of a Si substrate as a function of time during the laser irradiation (pulse duration: 23 ns) with different fluences ranging from 0.69 to 2 J/cm^2.

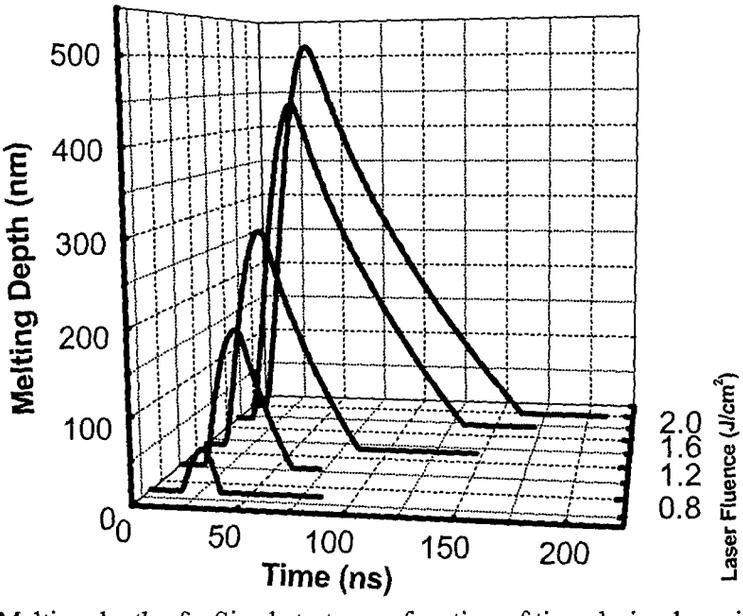

Figure 15. Melting depth of a Si substrate as a function of time during laser irradiation (pulse duration: 23 ns) with different fluences ranging from 0.69 to 2 J/cm^2.

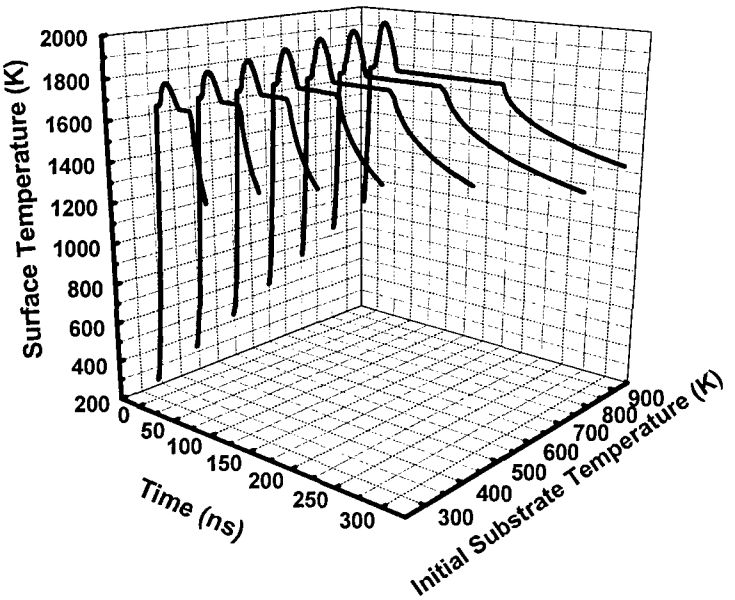

Figure 16. Surface temperatures of a Si substrate as a function of time with different initial substrate temperatures ranging from 300 to 900 K during the laser irradiation (pulse duration: 23 ns) with a fluence of 1 J/cm^2.

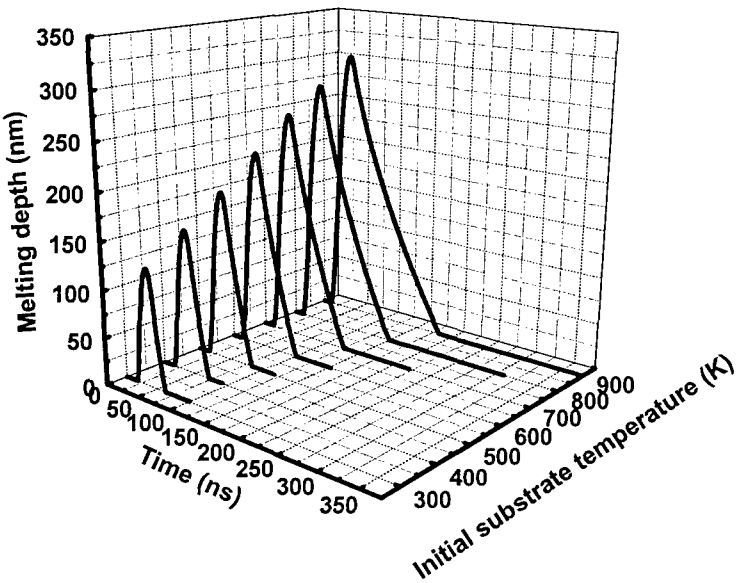

Figure 17. Melting depths of a Si substrate as a function of time during the laser irradiation (pulse duration: 23 ns) with a fluence of 1 J/cm^2 and with different initial substrate temperatures ranging from 300 to 900 k.

2.3 Dual size self-assembly and imprinting

We investigated dual-size self-assembly using several combinations of different sized silica particles into regular patterned assemblies. In particular, we used self-assemblies of dual size

particles with large size ratios to produce hexagonally close-packed monolayers. Figures 18(a)-(d) show the dual size self-assemblies of silica particles with different diameter ratios and SEM magnifications. Figures 19(a) and 19(b) show the structures formed after laser imprinting.

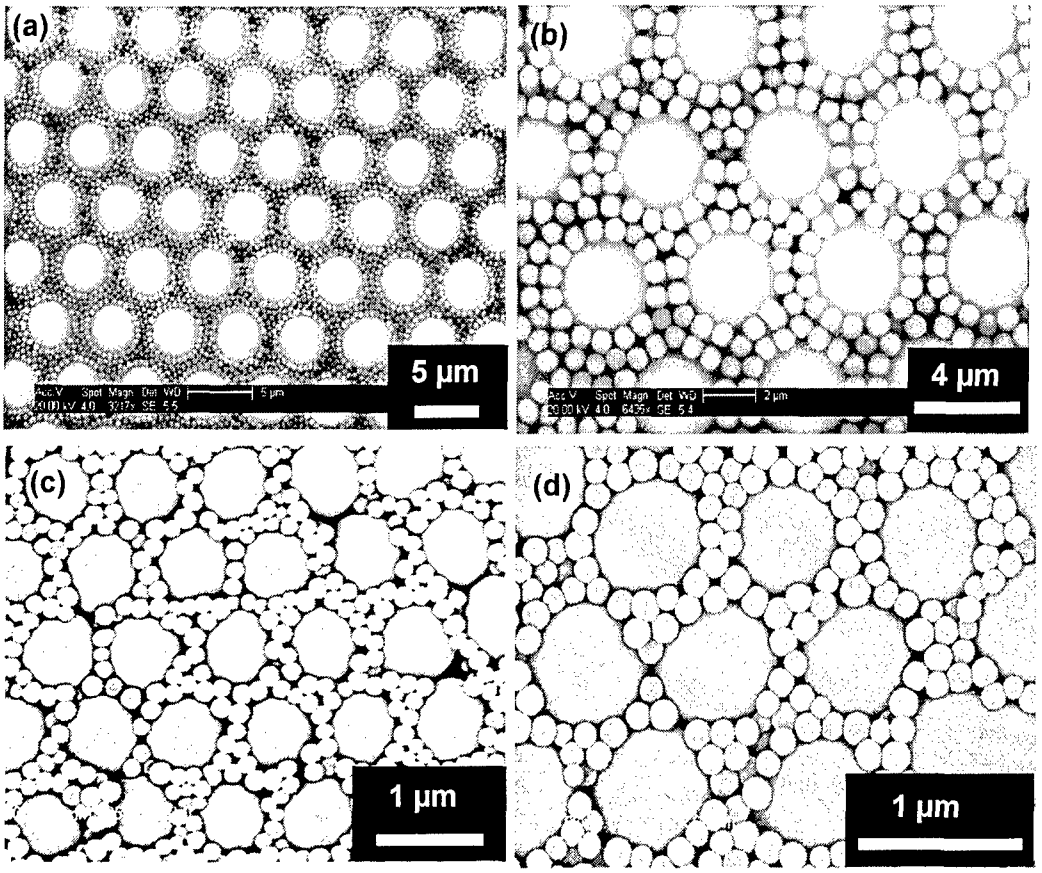

Figure 2-16 Dual size self-assemblies of particles with different size combinations:(a) 5.06 and 0.49 µ m: (b) 5.06 and 0.49 µ m (c) 0.97 and 0.16 µ m (d) 0.97 and 0.16.

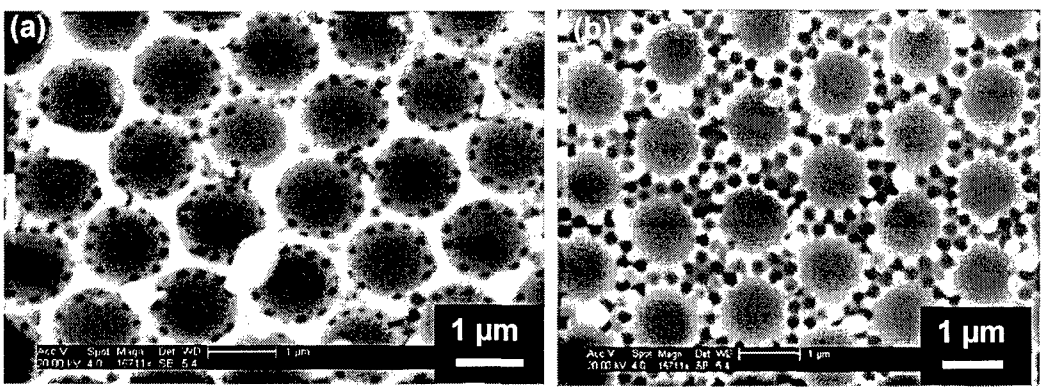

Figure 2-17 Periodic structures which were fabricated laser-assisted nanoimprinting of dual-size self-assembled silica particles of 1.54/0.3 µm with a fluence of 1 J/cm2: (a) smaller cavities covered by melted silicon which was pressed out from the cavities during the imprinting process; (b) bigger cavities at the center closely encompassed by smaller cavities.

3. Laser–assisted chemical vapor deposition for fabrication of PBG structures

The process to fabricate PBG structures using laser-assisted chemical vapor deposition (LCVD) consists of three steps: multilayer self-assembly of silica particles, LCVD, and HF etching. Figure 18(a) shows the schematic diagram of the experiment setup for LCVD. Figures 18(b)-(g) illustrate the whole processing procedure, step by step. After each processing step, the structures were characterized by SEM. Raman spectroscopy (RS) was performed to determine the quality of the silicon films deposited by LCVD.

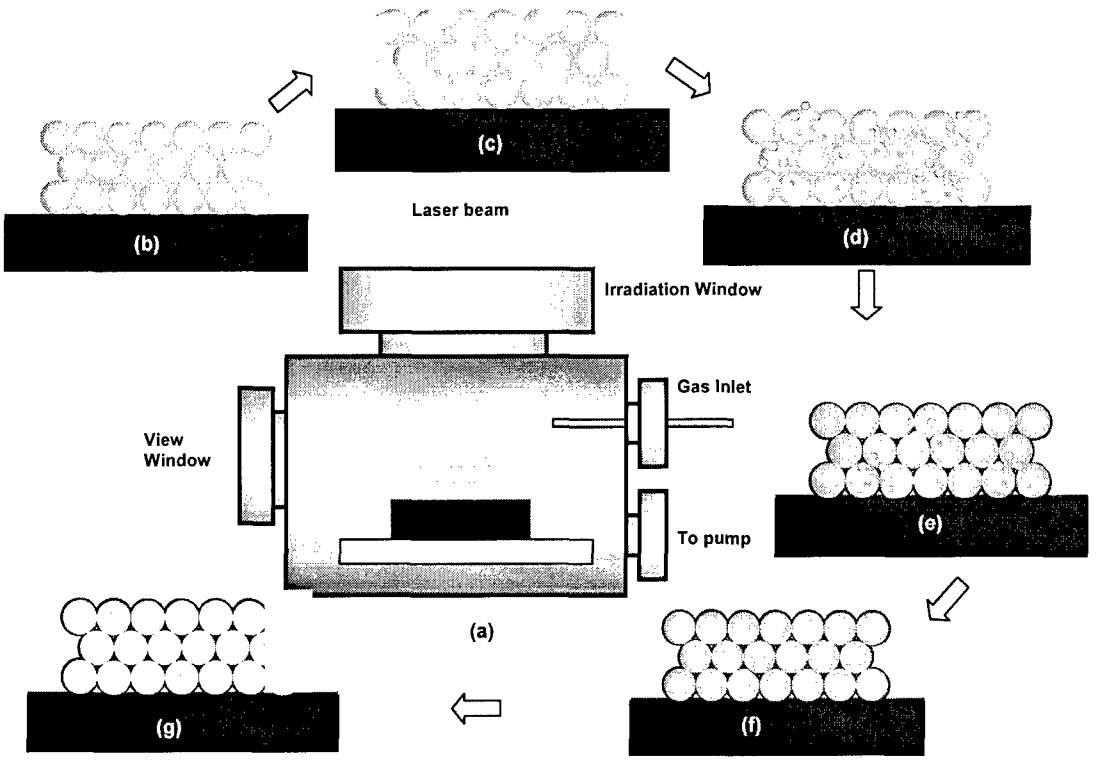

Figure 18. (a) Schematic diagram of LCVD system; (b) Self-assembly of silica particles; (c) Silica particles in a chamber with gas precursors; (d) thermal decomposition o gas molecules under laser irradiation; (e) CVD process; (f) spherical silicon shells covering silica particles; and (g) spherical silicon hollow shell array obtained after HF etching.

In order to predict the optical properties of the fabricated PBG structures, numerical simulations were carried out using the plane wave expansion simulation, transmission matrix simulation, and FDTD. The PBG structures were modeled as face center cubic (FCC) structure, illustrated in Fig. 19, with different geometry and refractive index.

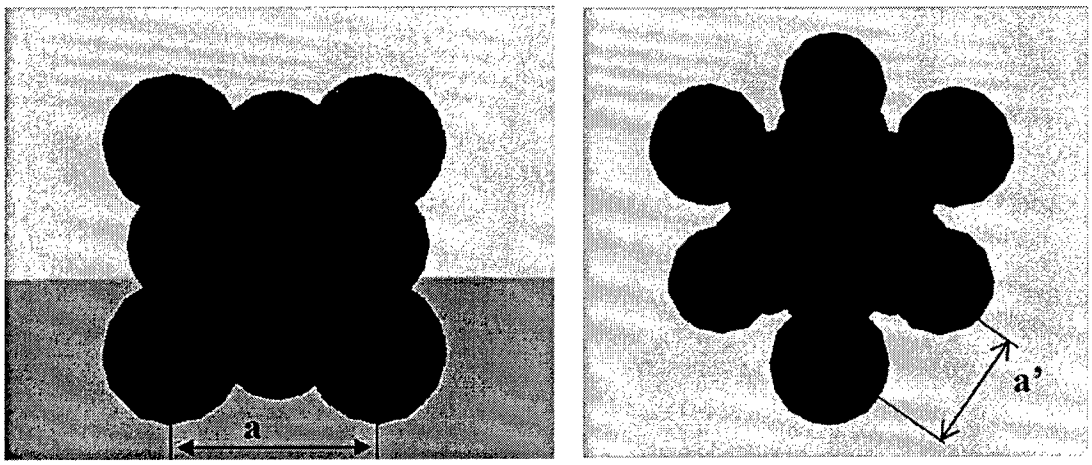

<100> Crystal plain of FCC **<111> Crystal plain of FCC**

Figure 19. FCC PBG Structure.

3.1 Multilayer self-assembly of silica particles

The isothermal heating evaporation-induced self-assembly (IHEISA) method was used to assemble the silica particles. Silica particle suspensions in ethanol (5~10% wt) were placed in a cylindrical glass vial. The cylindrical-shaped glass vials with a length-to-width ratio of 3.5:1 were used for vertical deposition. The vial with suspensions was placed in an oven (Fisher Isotemp Standard Lab Ovens) whose internal temperature was set as 79.5 °C. Silicon substrates were cleaved into 10 mm × 10 mm pieces along the crystal directions, cleaned by ultrasonic agitation in methanol, acetone and deionizer water subsequently for 5 min each. Then the substrates were put into the bath of freshly-prepared Piranha solution (H_2SO_4/H_2O_2, 7:3). Hydrofluoric-acid (HF) was then applied to remove the oxide film. After the substrates were rinsed thoroughly with deionized water and ethanol, they were ready for deposition. The substrates were held with paper clips, carefully centered in the vials. In order to prevent even trivial air flow in the oven which may impact the self-assembly, beakers were used to cover the vial. The ethanol suspensions were evaporated completely, leaving a shiny colloidal film on both the substrate and the vial wall. Figures 20(a)-(c) show the schematic of IHEISA deposition and the convection patterns. The schematic drawings of the top and side views of the silicon substrate with an assembly of multilayer silica particle film are shown in Figs. 20(c) and 20(d).

The monodisperse silica suspensions were heated isothermally at 79.5 °C, around the boiling temperature of ethanol. The silica particles were driven by the convection of ethanol. At the liquid-air surface, the ethanol evaporated fast without affecting the meniscus. After the complete evaporation of ethanol, typically in 3 to 4 hours for 5 ml dispersion, the self-assembly films were formed. Figures 21(a)-(c) show the top view of the multilayer assembly of 0.81 μm silica particles under different magnifications. Figure 21(a) shows the edge of the top layer, in which the uniform particle arrangement at the lower layer is presented. The insert of Fig. 21(a), which is a fast Fourier transform of the image, evidences the threefold symmetry characteristic of zone axis [111] in an FCC lattice. Figure 6(d) shows the cross section of the self-assembly, indicating

that the particle layers were stacked into ABCABC order which is the cubic close-packed structure, face-centered cubic as well. Wide area and uniform assemblies can be achieved.

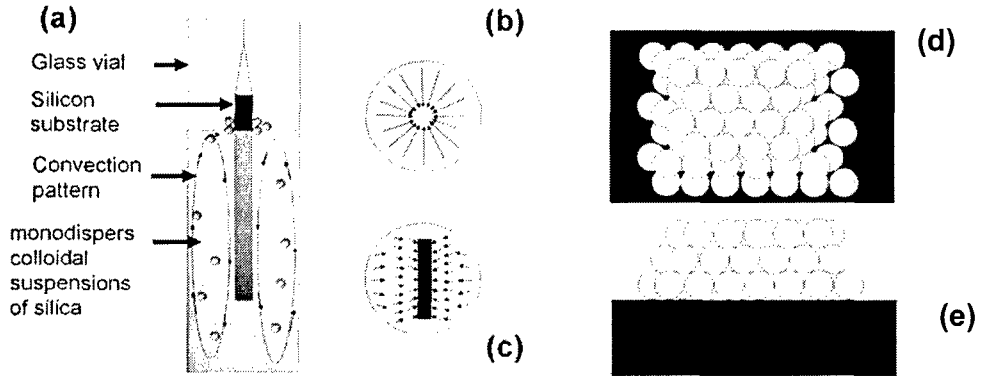

Figure 20. (a) Schematic of IHEISA colloidal crystal deposition. (b) Top view of convection pattern in a vial without sample. (c) Top view of convection pattern when silicon substrate is placed in the center of the vial. (d) Schematic of the top view of the self-assembled multilayer colloidal crystal on a silicon substrate. (e) Side view of the colloidal crystal.

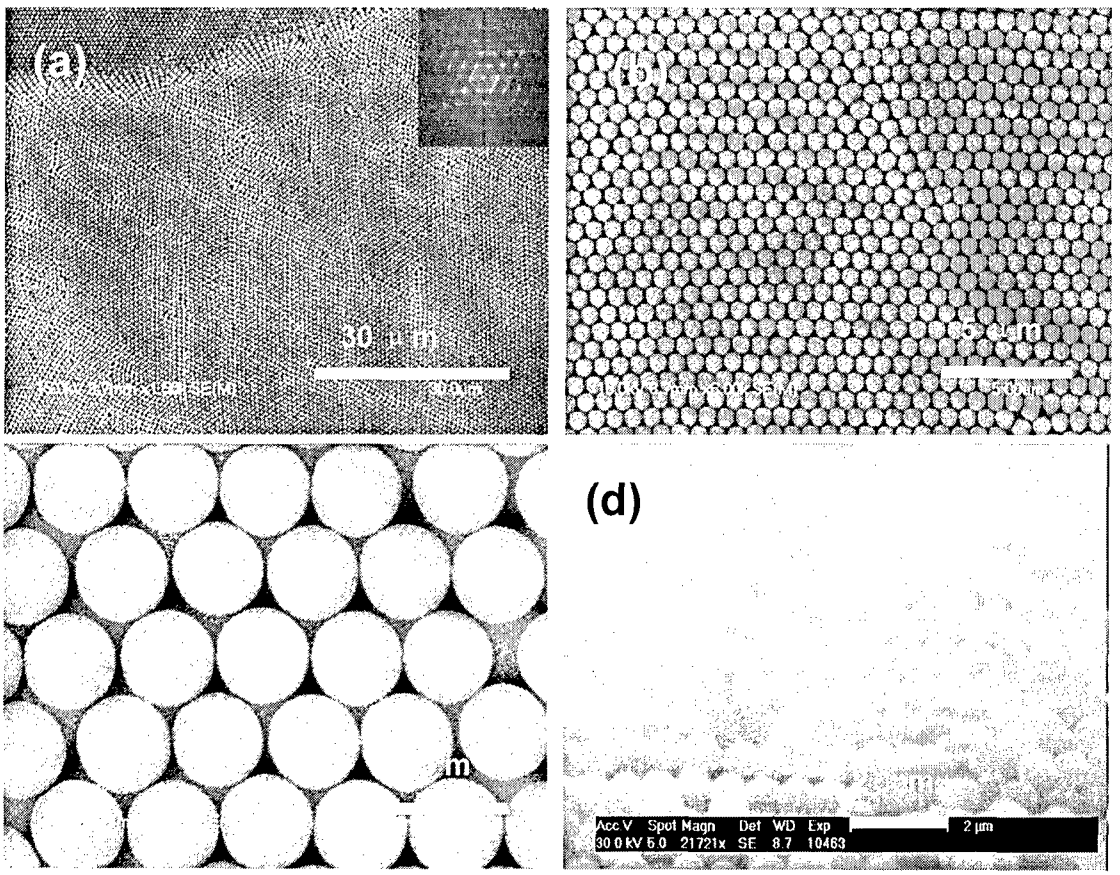

Figure 21. (a)-(c) SEM micrographs of the multilayer assemblies of 0.81 μm silica particles on silicon substrate. (d) The cross-section of the multilayer self-assembly.

In order to characterize the optical properties of the PBG structures of the colloidal crystals, ellipsometry was used to characterize the reflection of the self-assembly films on silicon substrates.

Although the contrast in the refractive indices between silica and air is not large enough to form complete bandgaps, the incomplete bandgaps located in the visible range may be observed directly by naked eyes. The multilayer self-assembled film with 0.33 μm silica particles could be observed in two different colors when observed from different angles, as shown in Figs. 22(a) and 22(b). It indicates that from certain incident angles, the green and red lights cannot propagate through the structure. Figure 22(c) shows the simulated photonic band structure of the FCC crystal (silica spheres, air background, sphere radius/lattice constant = 0.3535). It is clear that the left gap is just in the wavelength range of the green color and the right gap is just in the wavelength range of the red color.

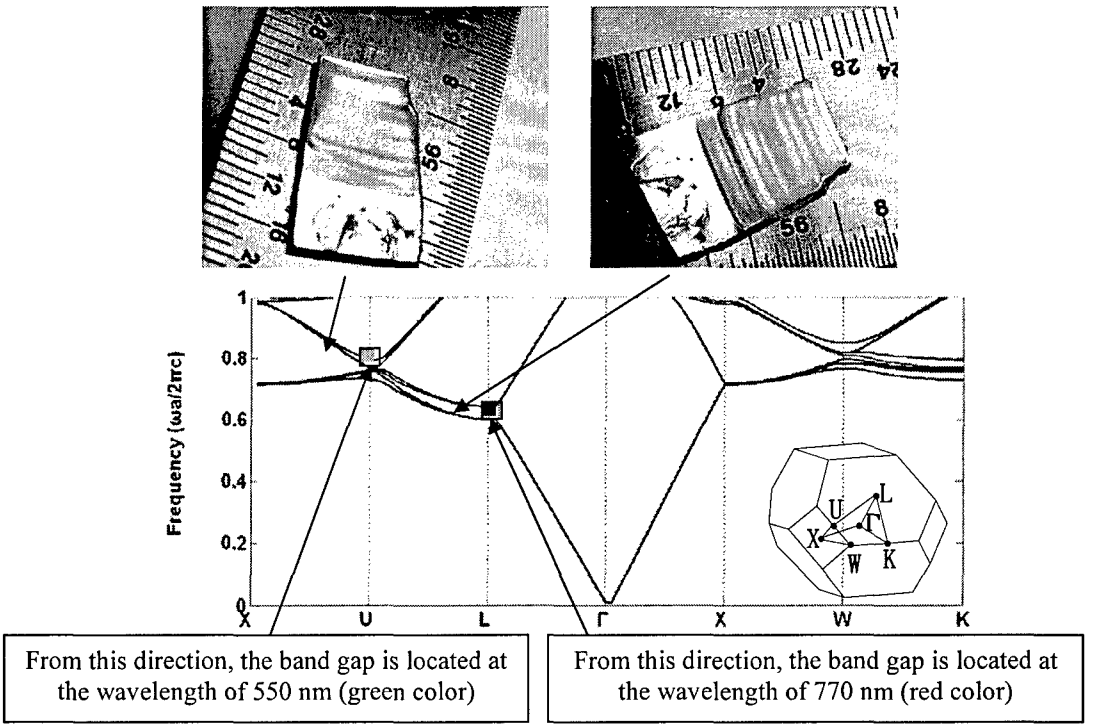

Figure 22. (a), (b) Pictures of a self-assembled film with 0.33 um silica particles taken at two different angles; (c) simulated photonic band structure of the FCC crystal with the self-assembled silica particles.

It is clear that the photonic bandgap of a colloidal crystal can shift if the observation direction is different. Figure 23 indicates the simulated PBG shift caused by the change in the incident angle. One specific incident angle is corresponding to a vector in the reciprocal lattice. The photonic dispersion relation along normal incidence to (111) plane of FCC structure (indicated as red arrows in Fig. 23) is labeled in the diagram as red band. When the incident angle is oblique (shown as the blue arrows), the corresponding vector in the reciprocal lattice is shifted which could be referred in the position of blue band in the dispersion diagram.

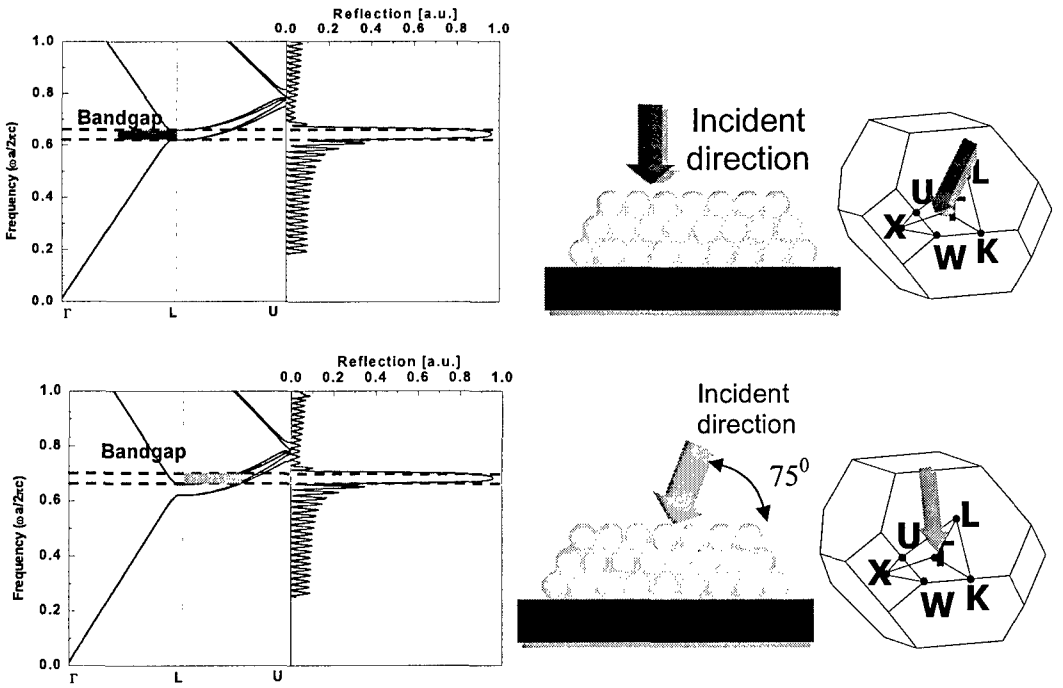

Figure 23. PBG shift caused by different incident angle.

The reflection spectrum of this PBG structure was simulated with the plane wave expansion method, transmission matrix simulations, and measured using a spectroscopic ellipsometer. The measured reflection spectrum is shown in Fig. 24 on the right (thick blue curve). The thin black curve is the reflection spectrum obtained from the transmission matrix simulation. The reflection peak at the shaded position in Fig. 24 is the pseudo PBG of the colloidal crystal, as shown in the left side of Fig. 24, which was obtained from the plane wave expansion simulation. The simulation and measurement results show good consistency which indicates that the PBG structure can be obtained by the self-assembly technique.

3.2 Laser-assisted chemical vapor deposition

LCVD is an attractive process for material growth. First of all, a variety of materials, such as metals, semiconductors, insulators can be deposited by LCVD, which can also be applied to the fabrication of 3-D PBG structures. Principally, there are two types of LCVD. One is based on direct optical chemical decomposition of reactant gases. The other is based on laser-induced thermal effects. The latter was used in this study. A laser beam locally created a hot area on the substrate surface where gas decomposition and solid deposition occurred. LCVD is a cold-wall process, in which the laser beam heats up the desirable area instead of the whole chamber or large substrate stage in conventional CVD techniques. Meanwhile, LCVD is a top heating process. The substrates are heated from above while they are heated from below or from both sides, so that the substrates remain in a relatively uniform temperature environment. LCVD is also a fast CVD process. The intensive energy of the laser beam could instantaneously heat the substrates to a desired temperature, under which both deposition and annealing can be achieved.

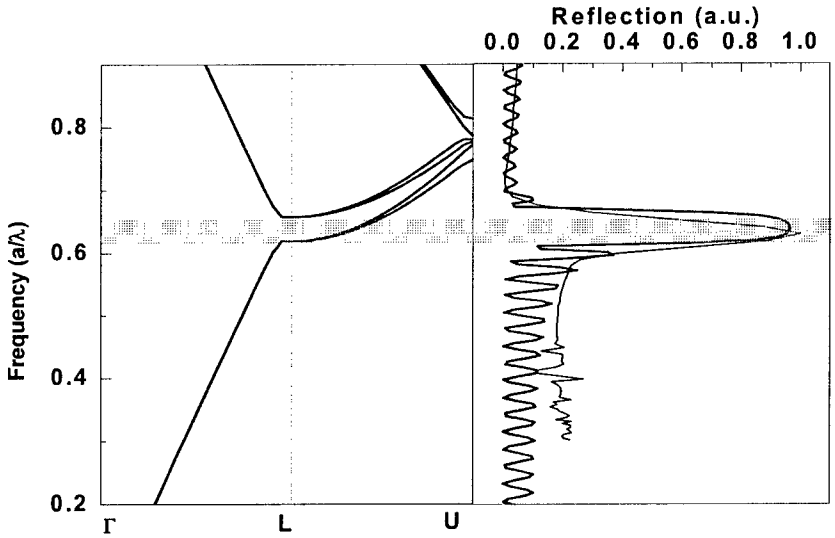

Figure 24. The photonic dispersion diagram of the PBG structure (left), and the reflection spectra (right) obtained from the simulation (thin curve) and measurement (thick curve).

Figures 25 and 26 show two setups of LCVD, using a carbon dioxide laser (10.6 μm, Synrad Inc., firestar v40) and a Nd:YAG laser (1064 nm, Quantronix Condor 200-IR), respectively. Both lasers were used to irradiate the substrates placed in a vacuum chamber. Due to the different absorptions of silica particles and silicon substrates to these two wavelengths, the deposition results were slightly different when the deposition thicknesses were larger than 20 μm.

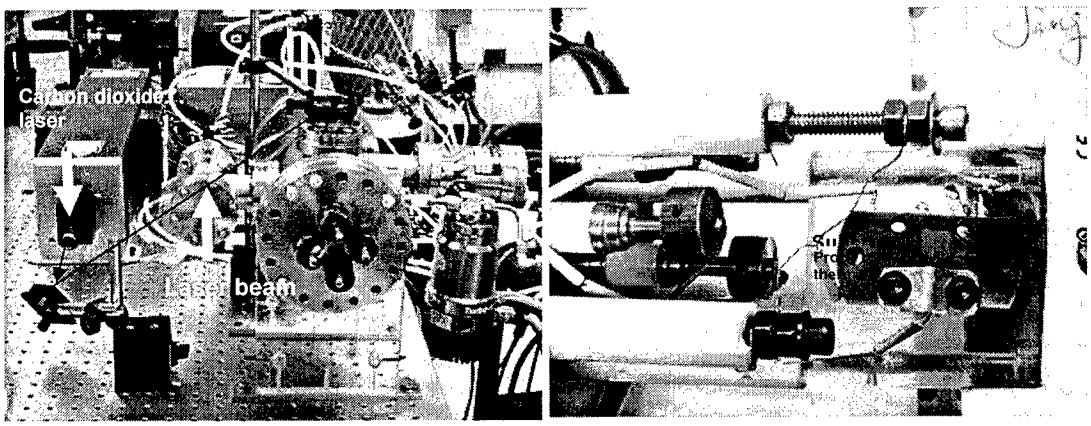

Figure 25. Experiment setup LCVD using a CO_2 laser.

The background vacuum pressure was 1×10^{-6} Torr. A laser beam first irradiated on the sample to heat it to 750~900 °C to remove the gas physically absorbed on the sample surface, before the precursor was filled into the chamber. After the degas process, disilane (Si_2H_6) (Voltaix Inc., 99.998 vol. %) was introduced into the chamber with an initial pressure of 200 mTorr. During the LCVD process, the laser power was kept unchanged. The temperature field was established instantaneously and a close-chamber CVD was initiated. Disilane was used as the only precursor in the LCVD process. As the reaction progressed, hydrogen was generated in the chamber. The hydrogen gas accelerated the reaction for silicon deposition. The LCVD process lasted for 1.5~3 min so that the deposited silicon could be infiltrated into the colloidal-crystal structures with a thickness of 10 to 20 μm. The high substrate temperature enabled not only rapid deposition, but also simultaneous annealing. Figures 27(a) and 27(b) show the structures after LCVD. The dents on each sphere are the points where the particle contacts with its neighbors. Figures 27(c) and

27(d) show the cross section of the structures, which could be used to determine the shell thicknesses.

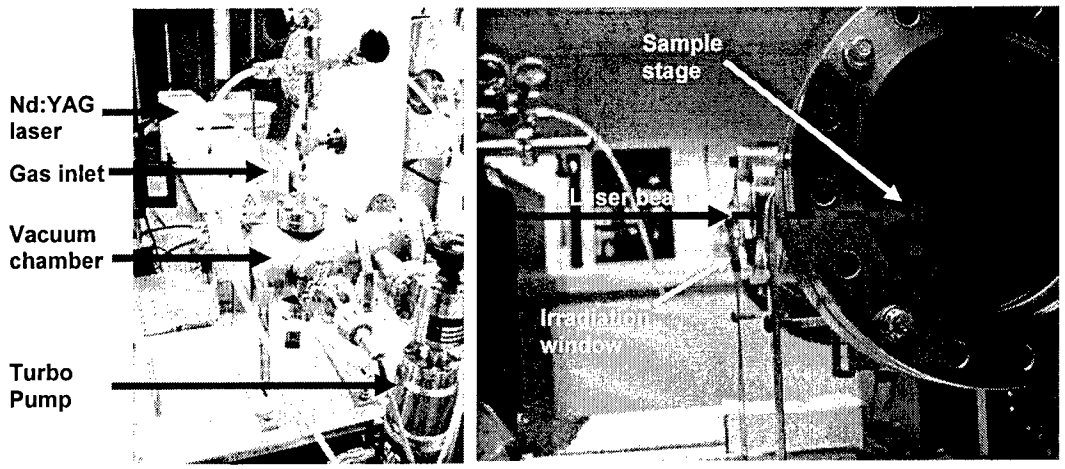

Figure 26. Experiment setup for LCVD using a Nd:YAG laser.

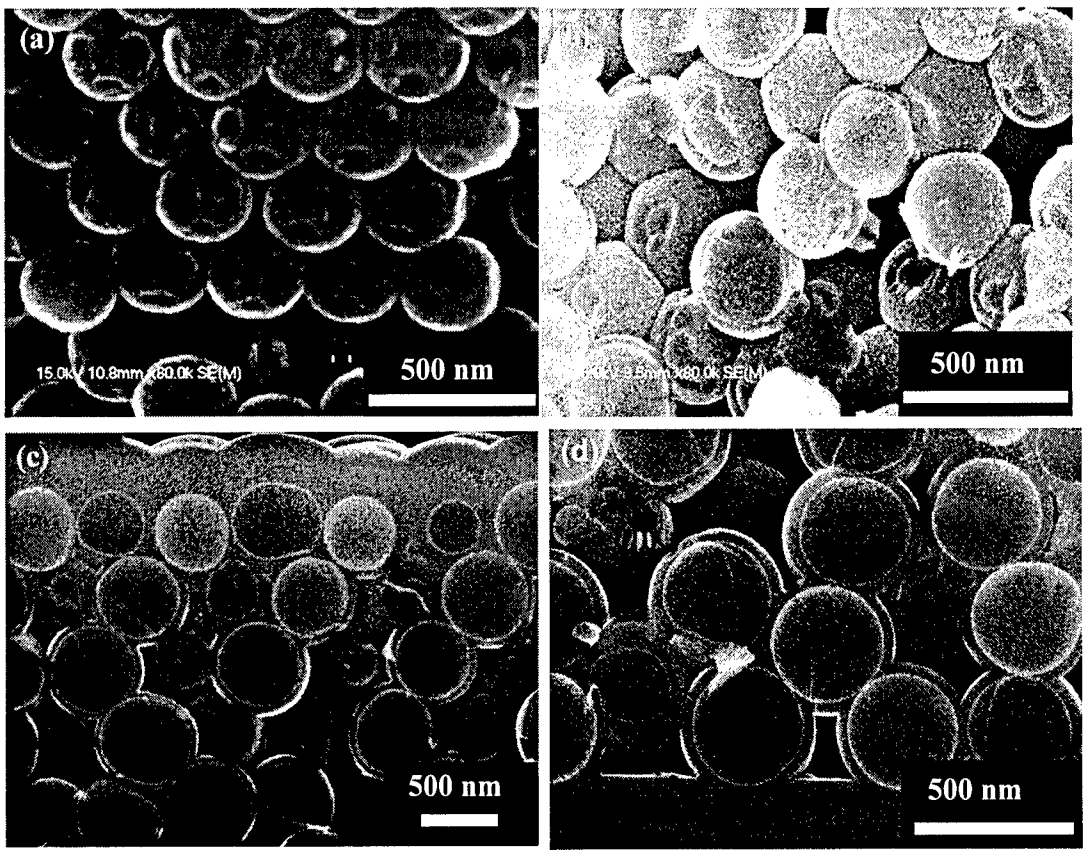

Figure 27. The SEM images of silicon shells covering silica particles under different magnitudes. (a-b) Side view of the silica core–silicon shell structure, (c-d) The cross section of the silica core–silicon shell structure.

These PBG structures were built up with the basic blocks of microspheres consisting of silica cores covered by spherical silicon shells (noted as silica@silicon). Figure 28(a) to 28(d) show the photonic dispersion diagrams simulated using the plain wave expansion simulation, corresponding to a group of silica@silicon structures with different core-shell ratios. Different shell thicknesses lead to different features in the PBGs. The shell thicknesses in the range of 5% to 20% radii were used in the simulations. The measurement using the silica@silicon in Figs. 27(c) and 27(d) indicated that the shell thickness obtained using LCVD was about 10% of the particle radii. The position of the measured PBG agrees with the simulation using for 10% shell thickness. This thickness value was used in the transmission matrix simulation. The simulated photonic dispersion diagram and the measured reflection spectrum are compared in Fig. 29, which shows the photonic dispersion diagrams of the PBG structure (left), and the reflection spectra (right) obtained from simulation (thin black curve) and measurement (thick blue curve).

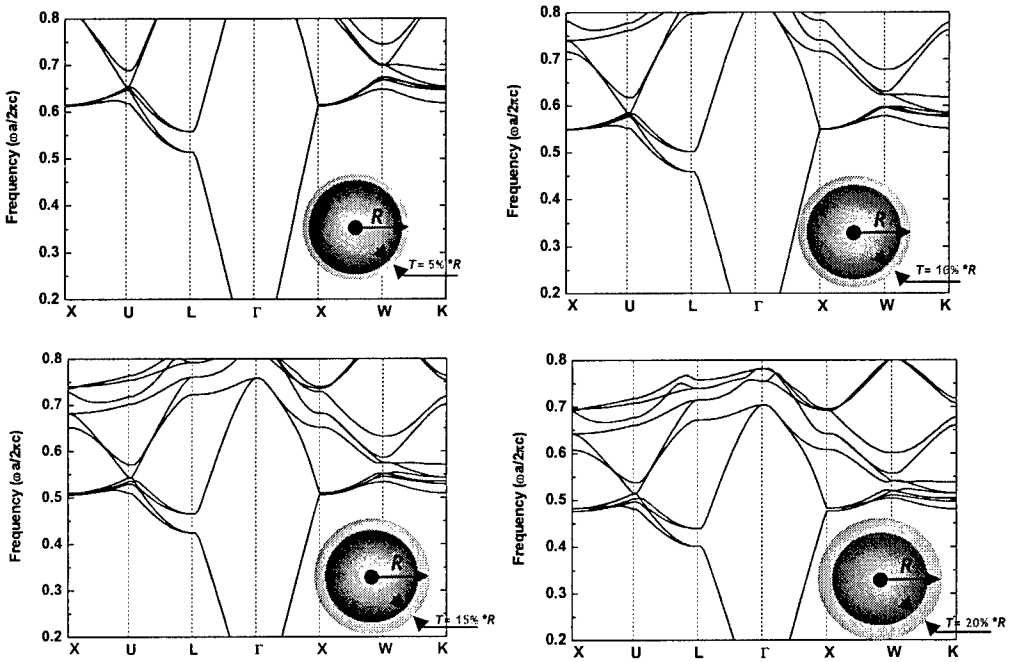

Figure 28. Photonic dispersion diagrams of silica core-silicon shell structures with different core-shell ratios.

Raman spectroscopy was performed to determine the quality of the silicon films deposited by LCVD. Two sets of samples prepared with different laser powers and durations were used, as listed in Table 1. Figure 30(a) is the Raman spectrum of sample A, which was deposited with a temperature below 800 °C. It is a typical Raman spectrum of amorphous silicon (a-Si). The two distinct bands at 180 and 500 cm^{-1} are associated with the transverse acoustic (TA) and transverse optical (TO) vibration modes, respectively. However, the Raman spectrum of sample B as shown in Fig. 30(b) has a sharp peak at 524 cm^{-1}, which indicates that the deposited film is crystal silicon (c-Si). The band at 980~1000 cm^{-1} is the second order Raman peak of silicon, associated with the high quality of the deposited crystal silicon. Due to the intensive energy provided by the laser beam, the deposition process progressed rapidly with annealing occurred simultaneously.

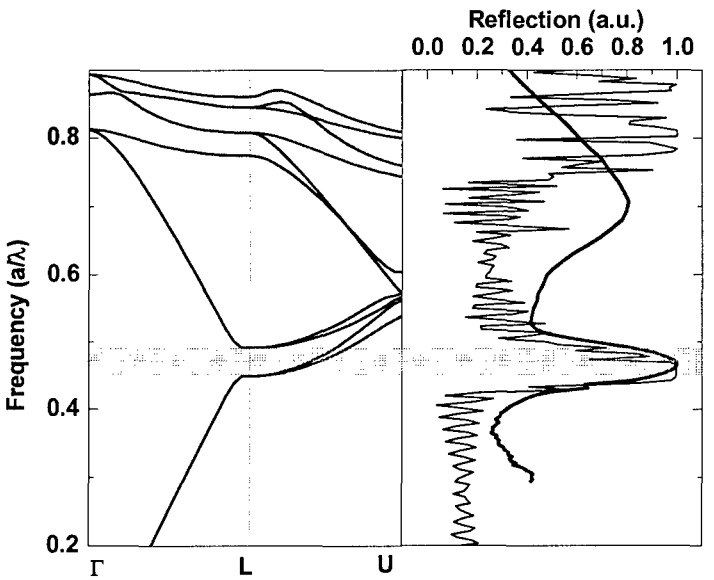

Figure 29. The photonic dispersion diagrams of the PBG structure (left), and the reflection spectra (right) obtained from simulation (thin black curve) and measurement (thick blue curve).

Table 1 Comparison of different LCVD conditions

Sample	Laser Power (W)	Substrate Temp (°C)	Deposition time (min)	Raman spectrum	Deposition
A	15	750	1.5	Fig. 3-6(a)	a-Si
B	20	870	3.0	Fig. 3-6(b)	c-Si

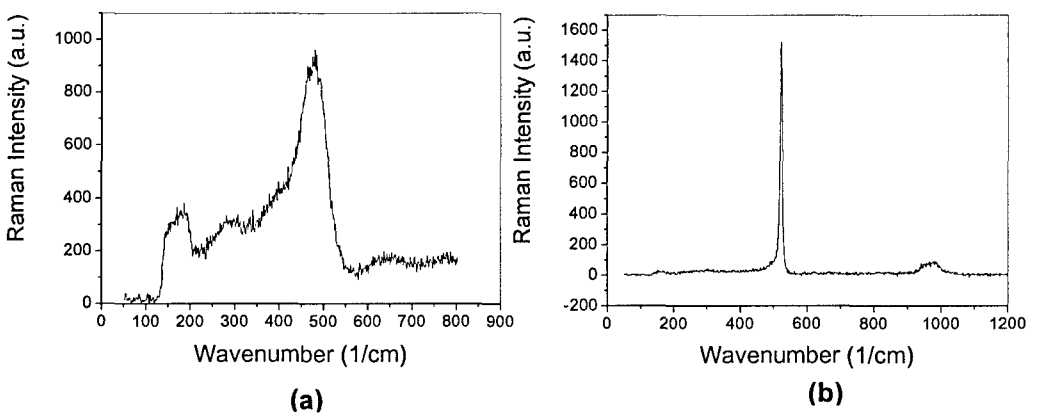

Figure 30. Raman spectra of the samples.

3.3 Spherical hollow silicon shell arrays

After HF etching, the silica cores in the silica@silicon structures were removed, leaving the hollow spherical silicon shell arrays. The structures are noted as air@silicon since they were the stacks of silicon shells with air cavities. These structures have larger refractive index contrast, which is easier to obtain complete PBGs. Figures 31(a) to 31(d) are the SEM micrographs of the PBG structures consisting of hollow spherical silicon shells.

Figures 32(a) to 32(d) are a group of photonic dispersion diagrams obtained from the plain wave expansion simulation. Different shell thicknesses provide different PBG features. The shell thickness of 10% of the particle radii result was used to compare with spectroscopic ellipsometer measurement of the PBG. The simulation results of photonic dispersion diagram and reflection spectrum were compared with measurement result in Fig. 33.

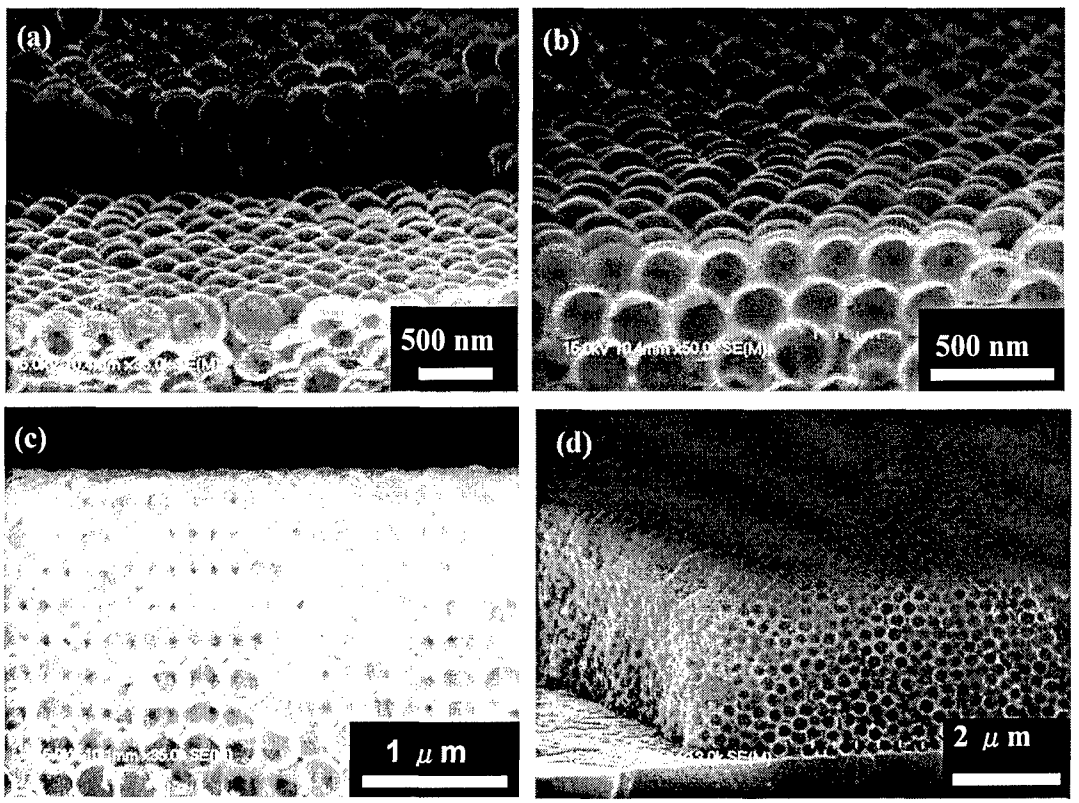

Figure 31. The SEM images of air@silicon PBG structures from different orientations and under different magnitudes. (a-b) The cross section of the air@silicon structure, (c) Cross section of the hollow spherical silicon shell, and (d) uniform PBG structure in a large area.

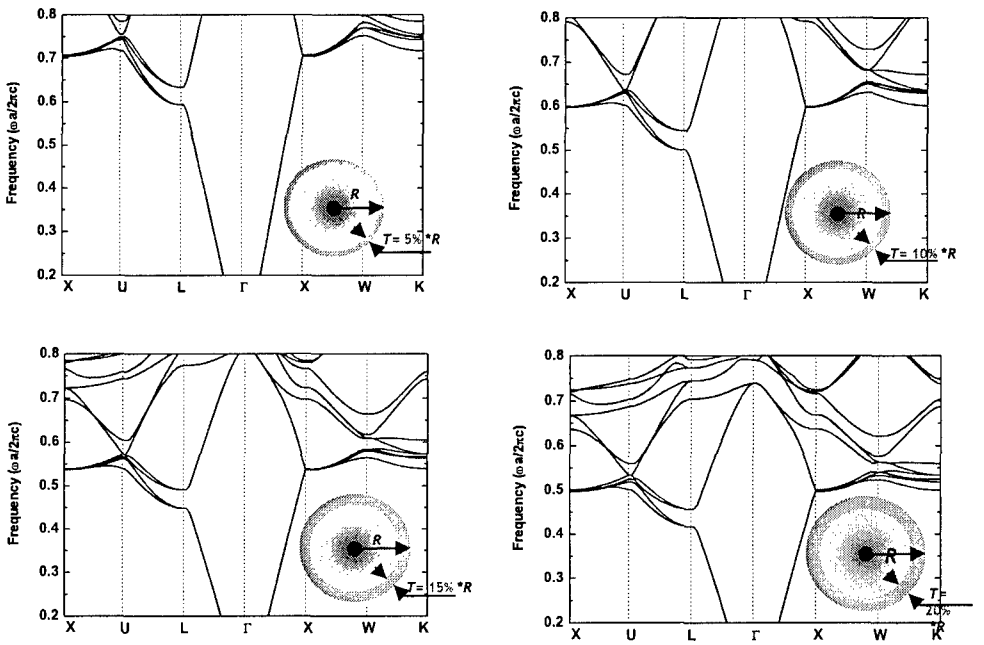

Figure 32. Photonic dispersion diagrams of air@silicon structures with different core-shell ratios.

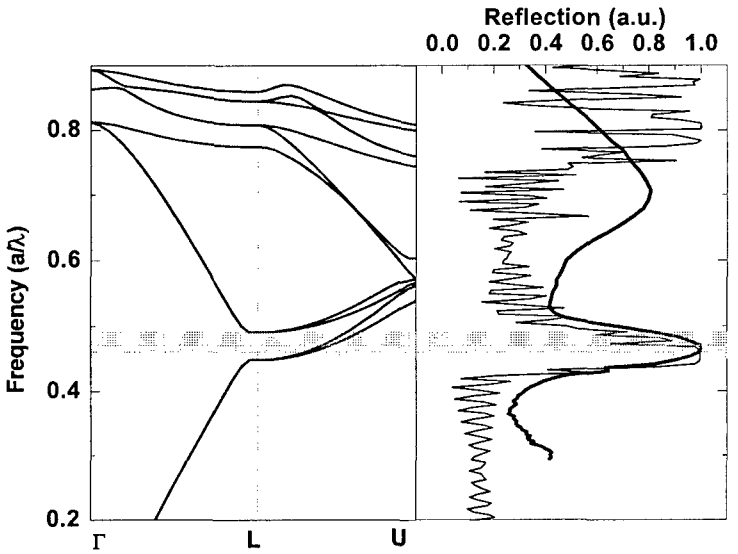

Figure 33. The photonic dispersion diagrams of the air@silicon PBG structures (left), and the reflection spectra (right) obtained from simulation (thin line) and measurements (thick line), for the structures

3.4 Finite difference time domain simulations

Finite difference time domain (FDTD) algorithm was used to simulate the behavior of 2-D PBG

structures. The simulations were carried out for 2-D PBGs only due to the limit of computing power. The simulated structure is 2-D PBG in silicon with closely-packed cylindrical cavities which is an analog structure to the 3-D air@silicon structures obtained in this study. The incident beams were set as plane waves. Figure 34 shows the electrical field distribution when the incident wavelength is not in the PBG. Figure 35 shows the case of in-PBG light propagation. Although the base material does not absorb the light (assumed in simulations), the optical wave in PBG is blocked. FDTD provides a clear description for the optical properties of the PBG structures.

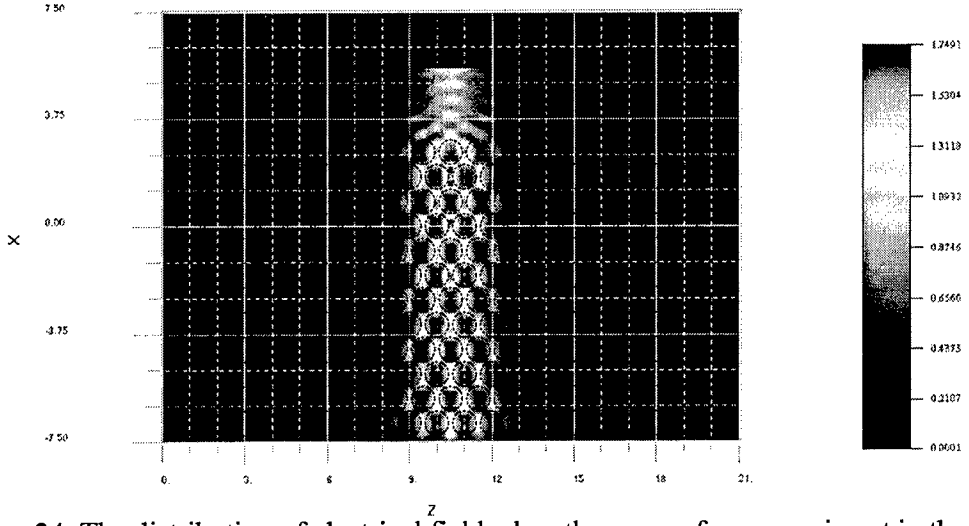

Figure 34. The distribution of electrical field when the source frequency is not in the photonic bandgap.

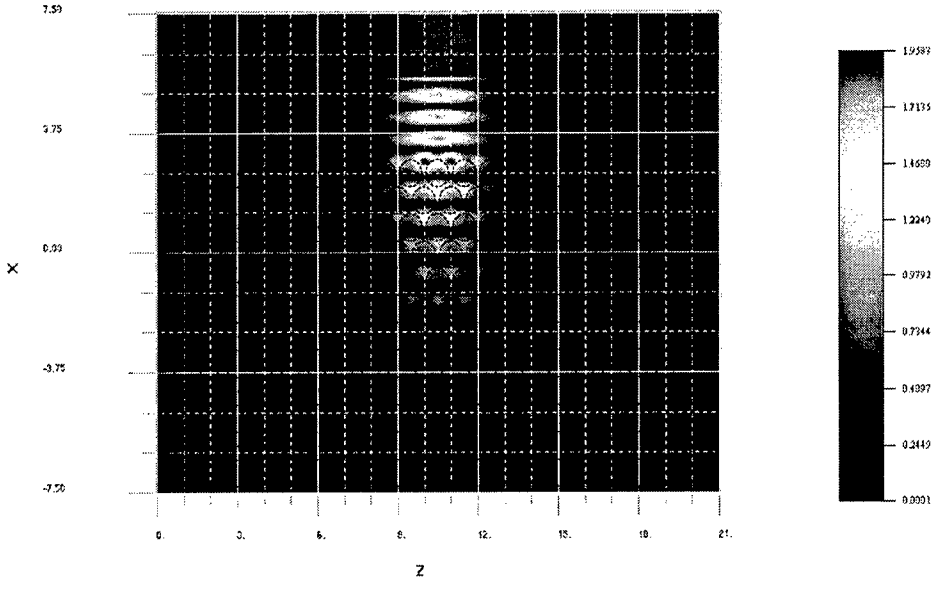

Figure 35. The distribution of electrical field when the source frequency is in photonic bandgap.

4. Conclusions

In the three years of the project period (Aug. 2003 ~ Aug 2006), we successfully fabricated the PBG structures using laser-assisted nanoimprinting and LCVD techniques. Figure 36 is the outline of our research achievements. Various PBG structures were fabricated. Thermal and optical simulations were carried out both to investigate the process mechanisms and predict the optical properties of the fabricated structures. The fabricated structures were also experimentally characterized to verify the consistency with the simulated results.

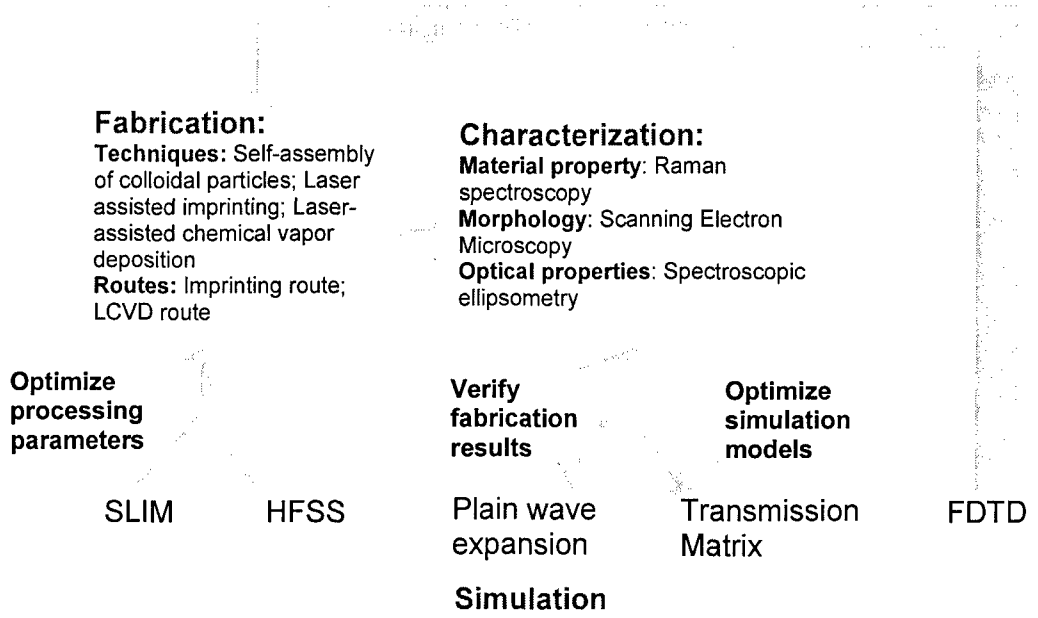

Figure 36. Summary of the project report.

Using laser-assisted nanoimprinting, 3-D PBG structures were fabricated using colloidal suspensions. Laser-assisted nanoimprinting is fast, simple and cost effective. The fabricated structures possessed three-dimensionality compared to its expensive counter parts. The numerical simulation using HFSS and SLIM were applied to exploring the mechanisms in the process.

Spherical silicon-shell PBG structures were fabricated using LCVD in combination with self-assembly of silica particles. The self-assembly technique yields large-area, high-quality PBG structures, which could also withstand high temperature in the silicon LCVD process. The LCVD process has the advantages of high intensity and highly localized heating for ideal thermal conditions. The process developed in this study allows us to deposit crystal silicon to infiltrate the colloidal crystals, which led to the fabrication of spherical-shell 3-D PBG structures. The spherical silicon-shell array structures could be optimized by varying precursor pressure and laser parameters. Hence, higher infiltration ratio of silicon could yield large and complete PBG.

5. Future work

In this project, the silicon-shell structures have been successfully fabricated. The silicon-shell structures fabricated in this project promise the infiltration of various functional materials, such as quantum dots or liquid crystals, for further research on functional PGB structure and devices. This opens the potential to fabricate electrically-tunable PBG crystals with integrated functionalities of positive refraction, negative refraction, and total reflection in a single material. (Fig. 37).

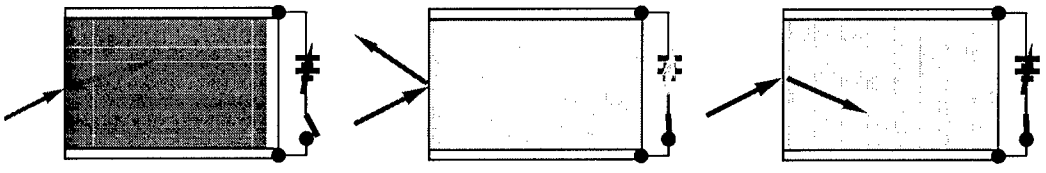

Figure 37. Schematic of electrically-functional PBGs.

In future research, liquid crystals will be filled into the PBG crystals to incorporate bandgap tunability. An external electrical field will be applied to control the refractive index of the liquid crystals, which leads to the displacement of the photonic band structures as shown in Fig. 38. As a result, the electrically-tunable PBG crystals will have different optical properties ranging from positive refraction to negative refraction and total reflection, depending on the external electrical field.

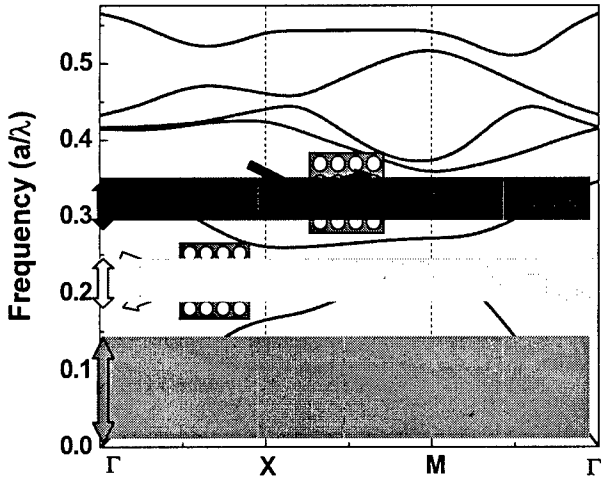

Figure 38. Photonic band structures.

Appendix

A1. Journal Papers

1. L.P. Li, Y.F. Lu, D.W. Doerr, D.R. Alexander, J. Shi, and J.C. Li, "Fabrication of hemispherical cavity arrays on silicon substrates using laser-assisted nanoimprinting of self-assembled particles", Nanotechnology, 15(3), 333-336(2004)
2. L.P. Li, Y.F. Lu, D.W. Doerr, D.R. Alexander and X.Y. Chen, "Parametric investigation of laser nanoimprinting of hemispherical cavity arrays", J. Appl. Phys., 96(9), 5144-5151 (2004)
3. L.P. Li, Y.F. Lu, D.W. Doerr, and D.R. Alexander, "Laser-assisted Nanopatterning of Aluminium Using Particle-induced Near-field Optical Enhancement and Nanoimprinting", Nanotechnology, 15, 1655-1660 (2004)
4. K.K. Mendu, J. Shi, Y.F. Lu, L.P. Li, N. Batta, D. W. Doerr and D. R. Alexander, "Fabrication of multi-layered inverse opals using laser-assisted imprinting", Nanotechnology, 16, 1965-1968(2005)
5. H. Wang, K.K. Mendu, Y.F. Lu, J. Shi, D.R. Alexander and D. W. Doerr, "Laser-assisted fabrication of 3-D structures on polymer films", J. of Laser Micro/Nanoeng. 1(2), 106-110(2006)
6. H. Wang, Z.Y. Yang, Y.F. Lu, "Spherical Silicon-Shell Photonic Bandgap Structures Fabricated By Laser-Assisted Chemical Vapor Deposition", submitted to J. Appl. Phys.

A2. Conference Papers and Presentations

1. L.P. Li, Y.F. Lu, D.W. Doerr, D.R. Alexander, J. Shi and K.G. Zhu, "Fabrication of Hemispherical Cavity Arrays on Silicon Substrates Using Laser-Assisted Nanoimprinting", Laser Microfabrication Conference, ICALEO 2003 (22nd International Congress on Applications of Lasers and Electro-Optics, 13-16 October 2003, Adam's Mark Hotel, Jacksonville, Florida, USA)
2. Y.F. Lu, L.P. Li, K.K. Mendu, J. Shi, D.W. Doerr, D.R. Alexander, Invited talk, "Fabrication of 2-D and 3-D Photonic Bandgap Structures Using Laser-assisted Imprinting of Self-assembled Particles", Symposium R: 3D Nanoengineered Assemblies, MRS Spring Meeting 2004 (Materials Research Society, 12-16 April 2004, San Francisco, USA)
3. L.P. Li, Y.F. Lu, K.K. Mendu, D.W. Doerr, D.R. Alexander, "Laser-Assisted Nanoimprinting Using Self-Assembled Nanoparticles on Silicon Substrates", 2004 Annual Meeting of the Nebraska Academy of Science (NAS) Aeronautics & Space Science Section (16 April 2004, Nebraska Wesleyan Campus, Lincoln, NE)
4. L.P. Li, Y.F. Lu, K. K. Mendu, D.W. Doerr, D.R. Alexander, "Laser-assisted nanoimprinting using self-assembled nanoparticles", Conference on Lasers and Electro Optics / Quantum Electronics and Laser Science Conference (CLEO/QELS 2004, 16-21 May 2004, Moscone Center West San Fracisco, CA, USA)
5. Y.F. Lu, "Laser nanoprocessing", Keynote Talk, Laser Microfabrication Conference, ICALEO 2004 (23rd International Congress on Applications of Lasers and Electro-Optics, 4-7 October 2004, San Francisco, CA, USA)
6. K.K. Mendu, Y.F. Lu, L. P. Li, D. W. Doerr and D. R. Alexander, "Fabrication of 3-D photonic bandgap structures on silicon using laser assisted-nanoimprinting", Laser

Microfabrication Conference, ICALEO 2004 (23rd International Congress on Applications of Lasers and Electro-Optics, 4-7 October 2004, San Francisco, CA, USA)

7. K. K. Mendu, Y.F. Lu, L. P. Li, D. Doerr and D. Alexander, "Laser Assisted Multiple Layer Nanoimprinting In Silicon Substrates", Symposium on Microscale and Nanoscale Laser Materials Processing (Society of Engineering Science Annual Meeting 2004, 10-13 October 2004, Lincoln, Nebraska, USA)
8. H. Wang, K. K. Mendu, Y. F. Lu, J. Shi, D. R. Alexander, D. W. Doerr, "Laser-assited fabrication of 3-D structures on polymer film", The Sixth International Symposium on Laser Precision Microfabrication (LPM 2005, 4-8 April 2005, Radisson Fort Magruder Hotel and Conference Center Williamsburg, Virginia, USA)
9. Y.F. Lu, Invited talk, "Laser Nanofabrication beyond the Diffraction Limit", Photonic Applications, Systems and Technologies 2005 (Optical Society of America, 23-26 May 2005, Washington, DC), PThC3
10. H. Wang, Y.F. Lu, K. Mendu, D.S. Alexander, D. Dorr, "Laser-assisted imprinting of self-assembled nanostructure", Laser Microfabrication Conference, ICALEO 2005 (24th International Congress on Applications of Lasers and Electro-Optics, 31 October – 4 November 2005, Miami, FL, USA)
11. Y.F. Lu, Invited talk, "Laser-assisted nanoscale material processing", 2005 ASME International Mechanical Engineering Congress & Exposition (IMECE 2005, November 15-11, 2005, Orlando, FL, USA)
12. H. Wang, Y.F. Lu and Z.Y. Yang, "Fabrication, characterization and simulation of inverse opal 3-D photonic crystals using laser-assisted imprinting", Confernece on Laser-Based Packaging III in in LASE2006 (Photonics West 2006, 21 - 26 January 2006, San Jose Convention Center, California, USA)
13. H. Wang, Z. Y. Yang, Y. F. Lu, "Laser-assisted Fabrication of 3-D Photonic Crystals", The 7th International Symposium on Laser Precision Microfabrication (LPM 2006, May 16-19, 2006, Kyoto Research Park, Kyoto, Japan)
14. H. Wang, Y.F. Lu, and Z.Y. Yang, "Laser-Assisted Imprinting of Self-Assembled Nanostructures", MSEC2006 (2006 ASME International Conference on Manufacturing Science and Engineering, 8-11 October 2006, Ypsilanti, MI)
15. H. Wang, Y.F. Lu, Z.Y. Yang, "Fabrication, characterization and simulation of noval 3-D photonic bandgap structures fabricated using laser chemical vapor deposition", Laser Microfabrication Conference, ICALEO 2006 (25th International Congress on Applications of Lasers and Electro-Optics, October 30 - November 2, 2006, Scottsdale, Arizona, USA)

A3. M.Sc. Theses

1. L.P. Li, "Laser-assisted nanoimprinting of self-assembled nanoparticles on semiconductor and metallic surfaces", University of Nebraska-Lincoln, July 2004
2. K. K. Mendu, Fabrication of 3-D photonic bandgap structures using laser assisted imprinting of colloidal silica particles", University of Nebraska-Lincoln, July 2005